ADVANCED THERAPEUTICS
www.advtherap.com

Advancements in Cancer Research: 3D Models, Single-Cell, and Live-Cell Techniques for Better Insights

Federica Carnevali, Stefania Forciniti, Valentina Onesto, Anna Chiara Siciliano, Helena Iuele, Giuliana Grasso, Anderson Fraga da Cruz, Ilaria Serra, Norma Depalma, Stefano D'Ugo, Prisco Piscitelli, Marcello G. Spampinato, Giuseppe Gigli, Carolina Camargo de Oliveira, and Loretta L. del Mercato**

The present review provides a comprehensive overview of the current state of in vitro cancer studies, focusing on recent advancements and ongoing in cell culture models and analyses techniques. Cancer cells grow in a complex and dynamic environment, interacting with various cellular components, such as stromal cells, cancer-associated fibroblasts, immune cells, and the extracellular matrix (ECM). The ECM provides structural support and unique characteristics essential for tumorigenesis. Accurately modeling this intricate tumor microenvironment and precisely analyzing cell–cell and cell–ECM interactions are crucial for understanding cancer progression and therapeutic responses. Consequently, oncology research is advancing toward a) three-dimensional tumor models, b) single-cell level analyses, and c) live-cell analyses. This review aims to elucidate current knowledge in this field, emphasizing the benefits these innovative approaches offer over traditional two-dimensional models, bulk analyses, and endpoint measurements.

1. Introduction

Cancer remains a significant global health threat. According to the International Agency for Research on Cancer (IARC), over 20 million new cancer cases are reported annually, with 9.7 million deaths in 2022. Projections suggest a 77% increase in cancer occurrences by 2050, amounting to over 35 million new cases worldwide.[1] Despite remarkable progress in understanding tumor complexity over the past 60 years, further research is needed to delve into the cellular and molecular determinants of cancer development, the mechanisms of cellular adaptation during tumor progression, and the quest for improved treatment options.[2–4] A critical obstacle in developing new anticancer drugs is the lack of valid and predictive in vitro cancer models. Few preclinical models effectively mimic the intrinsic complexity, heterogeneity, and spatiotemporal evolution of tumors.[5,6]

The tumor microenvironment (TME) is a continuously evolving system comprising a heterogeneous tumor cell population and other cellular components, such as endothelial cells, cancer associated fibroblasts (CAFs), mesenchymal stem cells, and immune cells.[7–9] These components are embedded in the extracellular matrix (ECM), a dense network of polysaccharides and proteins (e.g., collagen type I, fibronectin, and hyaluronic acid), providing structural support[10–12] and promoting cellular crosstalk through soluble factors such as cytokines, growth factors, and metalloproteases) [9,13]. The ECM

F. Carnevali, S. Forciniti, V. Onesto, A. C. Siciliano, H. Iuele, G. Grasso, I. Serra, G. Gigli, L. L. del Mercato
Institute of Nanotechnology
National Research Council (Cnr-NANOTEC)
c/o Campus Ecotekne, via Monteroni, Lecce 73100, Italy
E-mail: federica.carnevali@nanotec.cnr.it; loretta.delmercato@nanotec.cnr.it

F. Carnevali, A. C. Siciliano
Department of Mathematics and Physics "Ennio De Giorgi"
University of Salento
c/o Campus Ecotekne, via Monteroni, Lecce 73100, Italy

A. F. da Cruz, C. Camargo de Oliveira
Laboratory of Inflammatory and Neoplastic Cells, Department of Cell Biology, Section of Biological Sciences
Universidade Federal do Parana
Curitiba 81530-980, Brazil

N. Depalma, S. D'Ugo, M. G. Spampinato
Department of Surgery
"Vito Fazzi" Hospital
P.zza F. Muratore 1, Lecce 73100, Italy

P. Piscitelli
Local Health Authority ASL Le
"Vito Fazzi" Hospital
P.zza F. Muratore 1, Lecce 73100, Italy

G. Gigli
Department of Experimental Medicine
University of Salento
c/o Campus Ecotekne, via Monteroni, Lecce 73100, Italy

The ORCID identification number(s) for the author(s) of this article can be found under https://doi.org/10.1002/adtp.202400351

DOI: 10.1002/adtp.202400351

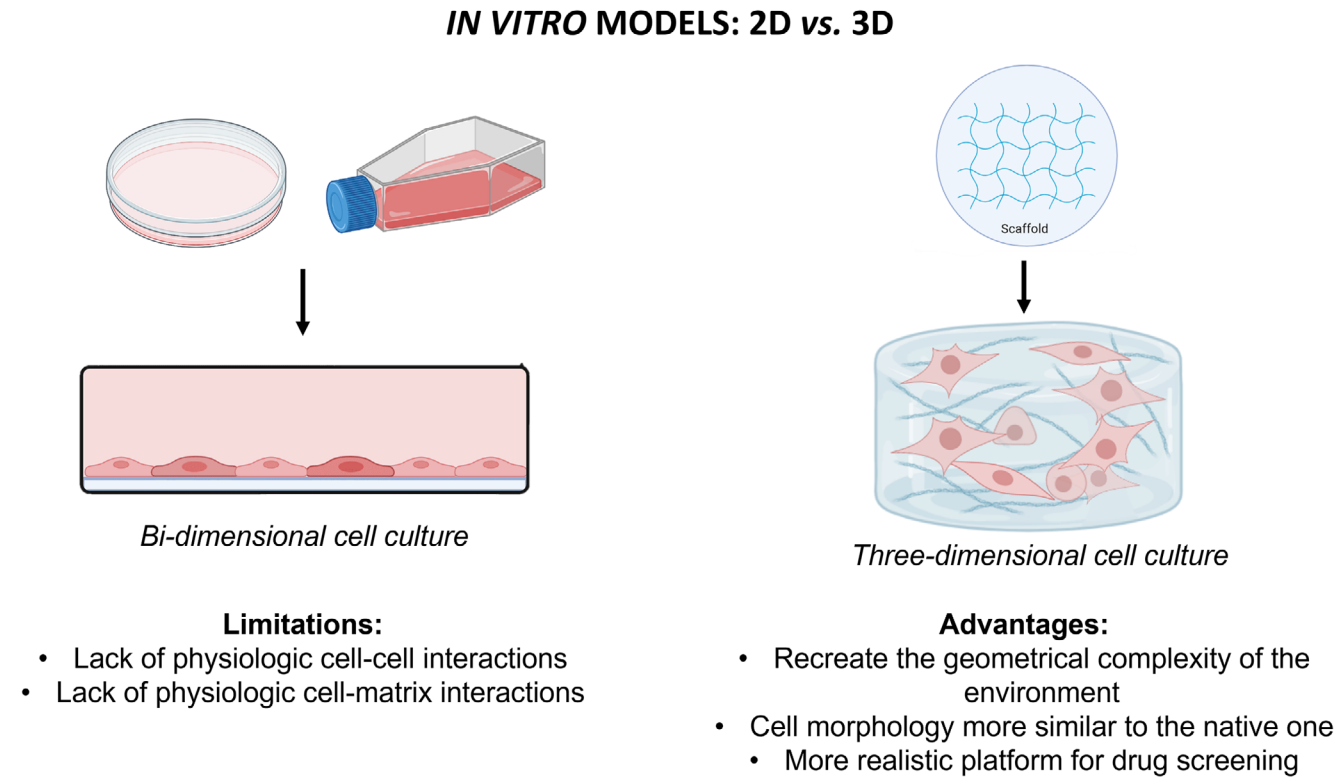

Figure 1. Schematic representation of the main differences between 2D (left) and 3D (right) in vitro cell cultures.

regulates cell–matrix interactions in a dynamic way, remodeling itself to support tumorigenesis,[14,15] disease progression,[7,13,16] metastasis,[17,18] and chemoresistance.[19,20]

Key hallmarks of the TME include hypoxia and acidification. Rapid tumor growth and poor vasculature create a hypoxic core, resulting in a metabolic switch known as the Warburg effect, where cancer cells rely on anaerobic glycolysis for energy production, leading to decreased microenvironment pH.[7,21–23] This metabolic shift influences the hypoxia inducible factor (HIF)-1α-signaling pathway, promoting angiogenesis to restore oxygen and nutrient supply and remove acidic metabolic waste.[24–27]

Precisely recreating this intricate and dynamic system, where various cell populations interact with each other and the environment, is crucial for advancing cancer research, particularly in the early stages of developing new therapies.

This review discusses the use of relevant in vitro tumor models to recapitulate the TME and highlights advanced technique for spatiotemporal analysis, crucial for understanding dynamic cell–cell and cell–matrix interactions and selecting effective treatments in preclinical drug development.

2. Comparative Analysis of 2D and 3D Models in Cell Cultures

2.1. Limitations of 2D Models

Since 1900s, two-dimensional (2D) cell cultures have represented the standard for studying cellular behavior and interactions.[28] These models are widely used to test drug efficacy and toxicity, develop vaccines, and understand human diseases, reducing the reliance on animal models.[28–30] However, 2D cultures have significant limitations as they fail to replicate the complex physiological and pathological conditions found in vivo.

2D cultures are cost-effective and easy-to-use, but they lack the ability to mimic the natural cellular microenvironment. Cells grow in a monolayer on a static, often rigid substrate, preventing them from adopting their natural morphology or forming complex cellular architectures. This limitation hampers cell growth due to enhanced contact inhibition and leads to epigenetic modification,[28,29,31,32] making these models less reliable for studying complex processes such as tumor invasion and metastasis.[28,33] Consequently, the pharmacological effects and transcriptome profiles observed in 2D cultures often do not correlate with clinical outcomes.[34,35]

In 2003, Alison Abbott's article "Goodbye, flat biology?" announced a new era in which three-dimensional (3D) cell systems emerged as a solution to these limitations.[36] **Figure 1** illustrates differences between these two approaches.

2.2. Importance of 3D Models

3D cell culture systems aim to closely mimic in vivo conditions, allowing for more cell–cell and cell–ECM interactions. These interactions are essential for replicating the complex communication networks that control cell morphology and functions, leading to more accurate disease modeling and preclinical drug screening.[28,37]

By better replicating geometric complexity of the microenvironment, 3D models enable scientists to study cell behavior under more natural conditions.[38] For cancer cells in 3D cultures can spontaneously arrange and grow into aggregates composed by multiple layers, creating oxygen and nutrients gradients similar to those in TME.[39] This structure also provides more accurate drug responses, as chemotherapeutic agents may diffuse differently within the 3D context compared to 2D models.[29,34,35]

3D cell cultures can be obtained using various methods, either with or without support systems, depending on the application.[28,30,40] The following sections summarize prominent techniques for generating 3D cancer models, classified into scaffold-free and scaffold-based constructs.

2.2.1. Scaffold-Free Constructs

Scaffold-free methods induce the self-assembly of multicellular clusters or spheroids without a supporting scaffold. Spheroids, which can range from 50 to 500 µm in size, can be composed of a single cell type or multiple cocultured cell types.[37,38] These spheroids replicate important features of solid tumor physiology, such as oxygen and nutrient gradients, and can form apoptotic–necrotic cores due to restricted nutrient diffusion.[6,37,39] This structure allows for the study of cellular interactions, proliferation, matrix production, and drug response within a 3D environment.[38,41]

Conventional scaffold-free approaches for spheroids generation include hanging drop, magnetic levitation, ultralow attachment plate, liquid overlay and liquid marbles (**Figure 2A**).[28,37,42,43] Each method has its own advantages and limitations in terms of spheroid formation efficiency and structural consistency.

The hanging drop technique uses surface tension and gravity to form size-controlled spheroids. The method consists in the production of small drops of cells/culture medium suspension on the lid of a Petri dish using a micropipette. The lid is then closed on the Petri dish containing water to prevent drying of the drops.[37] Due to the small working volume (≈20–40 µL), one critical limitation is the long-term maintenance of the spheroids in culture. To overcome this problem, in 2022, Jeong et al. proposed the use of a flipped deep-well plate to provide a higher working volume (over 1 mL per well).[43] Utilizing an overfilled 96-well plate, the authors succeeded in obtaining large human colorectal carcinoma cells (HCT116) self-assembled spheroids (over 1.5 mm in diameter), stable for over a month in culture, with high homogeneous morphology and sphericity. The as-obtained spheroids presented a necrotic core, different quiescent layers, and a highly proliferating periphery, mimicking in vivo solid tumor behavior (Figure 2B).

Magnetic levitation is reported as a rapid methodology to develop heterotypic spheroids uniform in size and shape. This technique uses magnetic nanoparticles and an external magnetic field to induce spheroid formation.[28] Onbas et al. developed a new setup to fabricate 3D cellular structures through magnetic levitation: the MagLev.[39] Cells suspended in high volumes (up to 800 µL), in presence of a nontoxic paramagnetic agent (Gadobutrol), assemble into spheroids in 24 h when a low external magnetic field is applied. Despite being an easy and rapid methodology, spheroid sphericity can be sensitive to cell type and concentration.

Other strategies for obtaining spheroids exploit the hydrophobicity of cell culture vessels. Ultralow attachment (ULA) plates, which are commercially available, feature a specific hydrophobic coating that reduces cell adherence and promotes self-aggregation. Similarly, low attachment plates can be customized using the liquid overlay technique (LOT). This method fosters spontaneous and rapid cells aggregation into spheroids by employing gels that has nonadherent properties, which prevent cell adhesion to the support. Comparing to ULA plates, the LOT technique does not require specialized equipment and is less expensive.[43] However, successful spheroid formation strongly depends on the cell's intrinsic ability to aggregate. Jubelin and colleagues demonstrated highly reproducible spheroid formation using the LOT method with various cancer cells lines, including lung adenocarcinoma (A549), prostatic adenocarcinoma (LnCaP), osteosarcoma (MNNG/ HOS), and glioblastoma (U251). In contrast, prostate adenocarcinoma (DU145, PC3) and colorectal adenocarcinoma (Caco-2, HT29) cell lines did not form spheroids after 10 days of culture.[29] Other studies have addressed this limitation by modifying the culture media or adding different exogenous ECMextracellular compound to improve aggregation. For instance, round prostatic adenocarcinoma (PC3) spheroids were obtained by growing cells with Matrigel,[44] while pancreatic (MiaPaCa-2) spheroids obtained with the addition of methylcellulose showed improved shape and long-term stability.[45] Another spheroid production method based on hydrophobic coating principle is the Liquid Marble (LM) technique, which uses hydrophobic powders to create microbioreactors for cell cultures. The cell suspension is dispensed onto a super-hydrophobic silica powder layer to form a droplet. By gently rolling the droplet, an even coating is formed, which impairs adhesion and allows cells to interact and self-assemble into spheroids in a short timeframe.[46,47] In a study by Langella et al., spheroids of C6 rat glioma cells (RGCs) obtained using hanging drops and the LM technique were compared.[48] While both methods replicated in vivo morphology and microtubular architecture, LM spheroids formed more rapidly. Additionally, markers of tumor plasticity, such as tyrosinated α-tubulin and acetylated α-tubulin, were enhanced in LM spheroids, indicating a higher maintenance of plasticity in glioma cells. To improve handling and avoid the use of powder coating directly on droplets, an advanced technique applies the hydrophobic coating directly to standard cell culture microplates, creating a Naked Liquid Marble (NLM) system for drug screening.[49] Super-hydrophobic surfaces were fabricated using the NeverWet Multi-Purpose Spray Kit (Rust Oleum) on commercially available 96-well microplates. In this platform, pancreatic adenocarcinoma cells (BxPC-3) successfully formed structures with high sphericity in less than 24 h. Treatment with nocodazole, an antineoplastic drug that inhibits microtubule polymerization, altered spheroid morphology and induced collapsing after 5 days (Figure 2C).

Overall, scaffold-free methodologies for generating tumor spheroids can replicate in vivo cell–cell interactions and de novo ECM deposition found in human solid tumors. These approaches have been particularly successful in creating 3D tumor models for various epithelial tissues, including lung, breast, prostate, and colorectal cancers. However, modeling nonepithe-

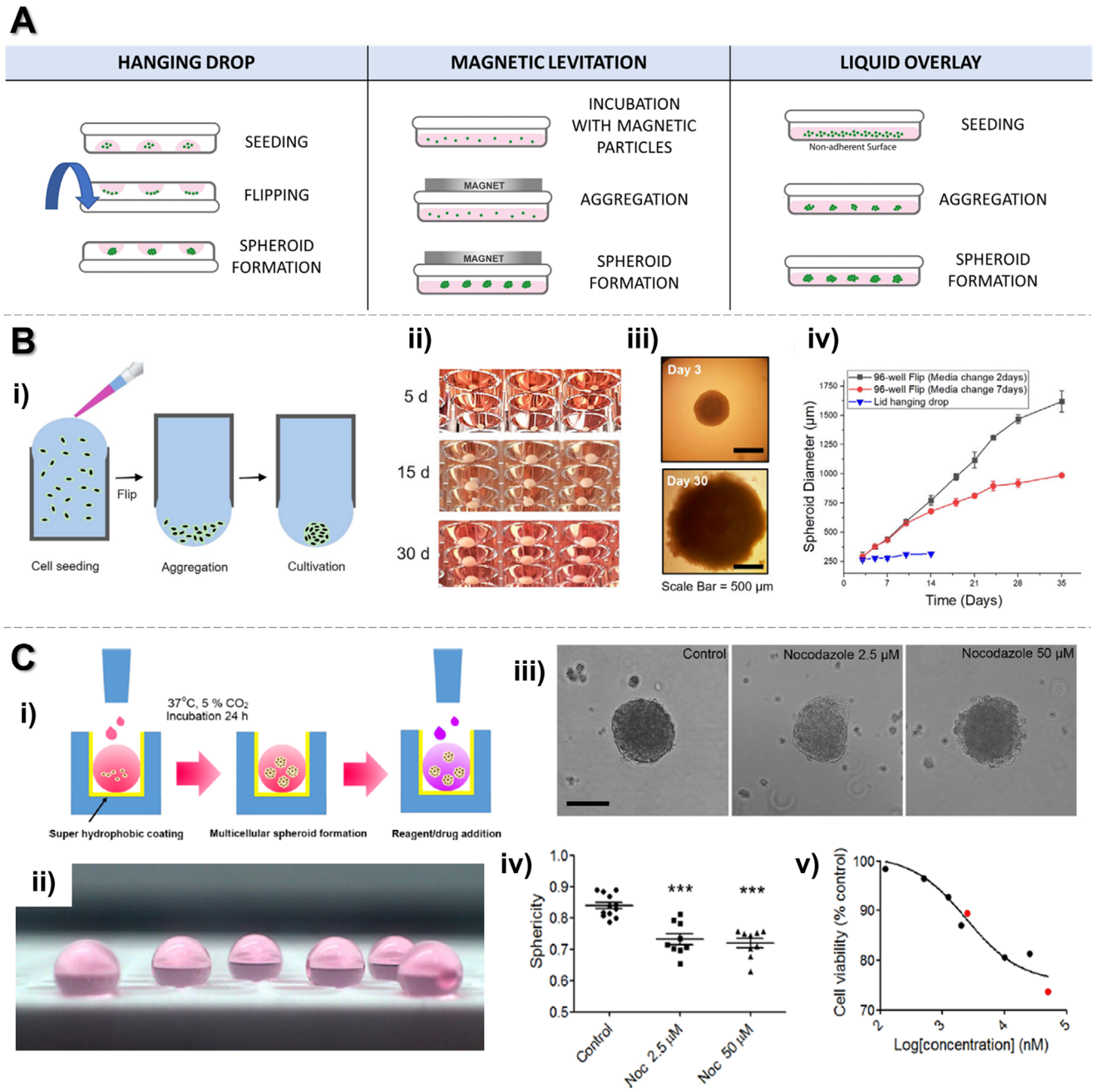

Figure 2. Examples of techniques to obtain 3D scaffold-free constructs. A) Schematic illustration of most used techniques for productions of cell spheroids: hanging drop (left), magnetic levitation (central), and liquid overlay (right). Adapted under terms of the CC-BY license.[37] B) – i) Schematic workflow of tumor spheroid generation by flipped deep-plate technique. ii) Images of 3D HCT116 spheroids long-term culture for 5, 15, and 30 days. iii) Microscope images of the spheroids at day 3 and 30. iv) Size measurement of HCT116 spheroid over 35 days. Spheroids obtained by traditional hanging drop technique (blue line) were compared to ones obtained by flipped deep-plate technique (black line: medium changed every 2 days, red line: medium changed every 7 days). Adapted under terms of the CC-BY license.[43] C) –i) Schematic workflow of spheroids formation and drug testing by NLM technique. ii) Image of NLMs on a superhydrophobic-coated surface. iii) Microscope images of BxPC-3 cell spheroids treated for 5 days with 2.5 and 50 µM nocodazole and without treatment (control). Scale bar: 100 µm. iv) Analysis of BxPC-3 spheroids sphericity after 5 days treatment with 2.5 and 50 µM nocodazole (Noc). v) Dose–response curve of BxPC-3 spheroids when treated with nocodazole. Adapted with permission.[49] Copyright 2019, American Chemical Society.

lial tumors, such as sarcomas, has proven more challenging due to the extreme heterogeneity of the TME in these cancers. This complexity makes it difficult to accurately replicate the diverse cellular and ECM components in scaffold-free spheroid models.[35,50,51] Since dense ECM deposition plays a crucial role in chemoresistance, these methods could serve as effective preliminary models for drug screening. However, emerging evidence suggests that cell–matrix interactions are critical during tumorigenesis and cancer progression. Thus, the absence of surrounding pre-existing ECM in spheroid assembly may fail to fully replicate TME.[6,52]

2.2.2. Scaffold-Based Approaches

Scaffold-based methods use biocompatible 3D structures to mimic ECM properties and support cell adhesion, proliferation, and migration.[30,40,53] These scaffolds can be made from naturally-derived or synthetic materials, and common forms include electrospun matrices, hydrogels, and 3D printed constructs.

Compared to scaffold-free approaches, scaffold-based methods offer significant in mimicking the interactions between cells and the ECM. These scaffolds not only provide structural support for 3D cultures, but also have the biophysical and biochemical properties that can strongly influence cellular behavior.[30,54] Additionally, scaffold-based systems can allow growth of a wider range of cancer cell lines, especially those that are unable to self-aggregate into stable 3D structures like spheroids or organoids. Furthermore, scaffold-based techniques are particularly suited for modeling malignancies in tissues with specific architectures or stiffness, such as bone, brain, bone marrow, and soft tissue sarcomas.[51,55–59]

Electrospun Matrices: Electrospinning (ES) is a cost-effective technique largely employed in tissue engineering to produce porous fibrous scaffolds that mimic the ECM. A charged polymeric solution is exposed to an electric field between a metal needle and a collector, kept at an optimized distance. When the applied electrostatic force overcomes fluid surface tension, a stable jet forms, and the fiber formation process begins.[60] Electrospun nanofibers can be obtained with diameters ranging from nanometers to sub-micrometers and are particularly suitable for cells requiring an aligned microenvironment, such as endothelial cells, osteocytes, myocytes, and neural cells.[61,62]

Electrospun scaffolds have been used to recapitulate the pathological ECM in cancer and investigate cell–ECM interactions. In particular, due to the versatility of this technique, researchers focused on cancers in which TME variations highly affect their development, migration, and chemoresistance.[63,64]

A study on triple-negative breast cancer (TNBC) used electrospun polylactic acid (PLA) scaffolds to assess a 3D model of the TME compared to traditional 2D cultures.[65] A 15% (w/v) PLA/chloroform solution was electrospun through a 24G needle to produce randomly oriented porous fibers with a diameter of 7 µm and a total thickness of ≈70 µm. Initially, MDA-MB-231 cells exhibited a lower proliferation rate in the electrospun scaffolds compared to monolayer cultures, which is typical in 3D environments. However, after 6 days, cell growth stabilized. The study found no differences in STAT3 gene activation, a marker related to self-renewal of breast cancer stem cells (BCSCs), but observed increased phosphorylation levels of the corresponding protein in the 3D culture condition. Through mammosphere-forming assay and RNA expression evaluation of epithelial-to-mesenchymal transition (EMT) markers, ES-PLA scaffolds were shown to enrich the BCSC population. The 3D model was validated for short-term breast cancer culture without significant BCSC-enrichment, indicating that few MDA-MB-231 cells undergo EMT in this environment.

The same polymer was used to create 3D models of colorectal adenocarcinoma in a comparative study with poly-ϵ-caprolactone (PCL), evaluating their mechanical properties in mimicking tumor tissue.[66] Electrospun fibers of both materials were produced with different collector configurations to adjust their size, alignment, porosity, wettability, and tensile mechanical properties. Caco-2 cells cultured on both scaffolds for 7 days demonstrated good viability. Metabolic activity in PLA scaffolds an increasing trend regardless of fiber alignment, whereas it decreased in PCL fibers and randomly oriented PCL fibers, as both scaffolds exhibited a Young's modulus in the range of 8–22 MPa and a strain at break of ≈70%, values close to the mechanical characteristics of large intestine.

Another application of this technique in cancer research focused on the morphological adaptation of human lung epithelial cell line A549 on electrospun polyvinyl alcohol (PVA)/Collagen nanofibers with tunable diameters and their consequent EMT-related gene activation (N-cadherin, vimentin, and fibronectin).[24] A549 cells grown on fibers with diameters of 170 nm showed up to fivefold upregulation in these genes compared to cells cultured on thinner (90 nm) and thicker (240 nm) fibrous mats (**Figure 3**A). The authors speculated that the scaffold's topological cues enhanced the EMT process in lung cancer cells, resulting in increased metastatic potential, and that this behavior was regulated by a specific range of fiber diameters. Consequently, fine-tuning the characteristics of electrospun fibers is necessary to produce robust in vitro cancer models that accurately represent both cell morphology and behavior.

In addition to the focus of this review, it is worth mentioning that ES plays an important role in cancer research as fabrication technique for drug delivery platforms. Indeed, the unique conformation of these scaffolds provides a high surface area-to-volume ratio, which favors the controlled release of antibiotics, anticancer agents, proteins, as well as nucleic acids.[67–70]

Hydrogels Scaffolds: Hydrogel scaffolds represent ideal platforms for 3D cell cultures due to their highly tunable biological, chemical, and mechanical properties which allow to recapitulate in vitro the TME hallmarks, particularly mimicking the native ECM.[31,33] Hydrogels are hydrophilic polymers that can be chemically or physically cross-linked and have the ability to retain a significant amount of water. During the cross-linking, the polymer undergoes a multidimensional extension of its chain, resulting in a 3D water-insoluble network structure.[71,72] These constructs can origin from natural or synthetic polymers. Naturally derived hydrogels represent the best option in terms of biocompatibility, maintaining cell viability and improving specific cellular functions.[71,73,74] However, batch-to-batch variations and uncontrolled biodegradation can lead to difficulties in controlling the mechanical properties and low reproducibility of commercially available hydrogel precursor, such as Matrigel.[75,76] In con-

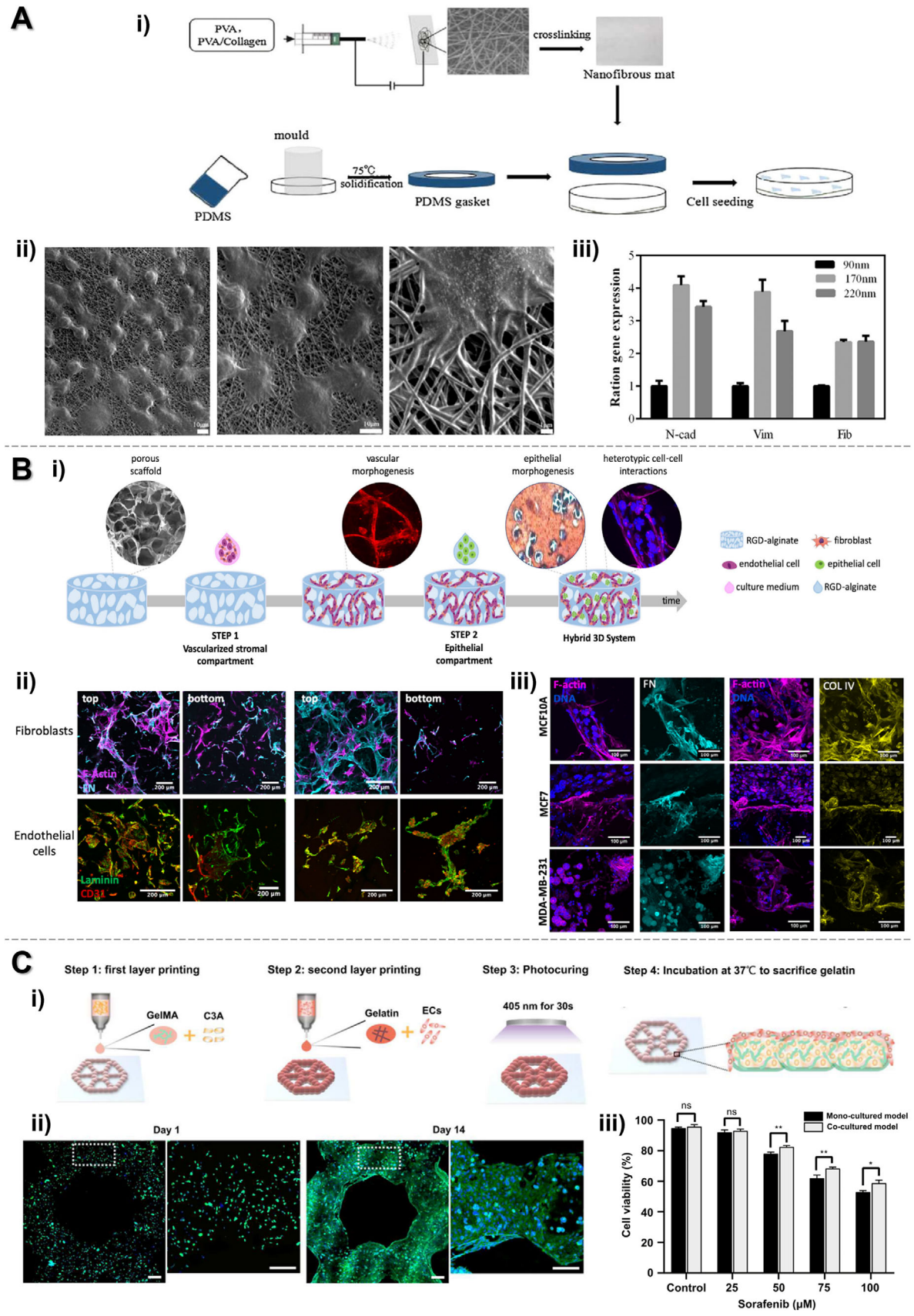

trast, synthetic hydrogels offer precise control over composition and mechanical properties, enabling the development of more reproducible 3D constructs with specific structures and physicochemical properties.[40,77] A major drawback of synthetic hydrogels is that, unlike native ECM, they do not provide extracellular cues and cell–matrix interactions. This limitation can be partially addressed chemically by introducing cell-binding and protease cleavage sites in the polymer.[71,78] Among the most commonly used hydrogels for 3D cancer model emerges alginate, a polysaccharide derived from marine brown algae. Alginate has numerous advantages, including a well-defined and xeno-free composition, adaptability of biochemical and physical properties, transparency for culture monitoring via optical microscopy, and easy cell recovery through chelating agents. Its most outstanding property is its ability to cross-link in the presence of divalent cations, most often Ca^{2+} ions[79–81] Bidarra et al. demonstrated that bioengineered arginine-glycine-aspartate (RGD)-modified alginate hydrogels can support epithelial cell morphogenesis into acini-like structures that reproduce functional and histological characteristics of native mammary tissue.[82] Using these 3D platforms, they were able to investigate EMT and its reversion (Mesenchymal-to-Epithelial Transition, MET) in EpH4 cells, shedding light on a mechanism with significant relevance to cancer progression and invasiveness. EMT-associated phenotypic alterations are highly correlated with cell–cell and cell–microenvironment interactions, such as loss of cell–cell adhesions, enhanced deposition of ECM proteins, and cytoskeleton alterations, which can only be observed and investigated using appropriate 3D models that mimic the TME. Another hallmark that can only be recapitulated within 3D models is angiogenesis, a complex process involving the interplay of epithelial cells, stromal cells (such as endothelial cells and fibroblasts), the ECM, and secreted factors.[34,83,84] To mimic the cooperative activities that these components in vitro, it is necessary to develop an engineered angiogenesis-promoting microenvironment that include an ECM-like 3D scaffold capable of supporting all these processes.

To address this challenge, Teixeira et al. developed an alginate-based heterotypic 3D breast model consisting of two compartments: i) a vascularized stromal compartment, i.e., a porous scaffold coseeded with fibroblast and endothelial cells, and ii) a parenchymal compartment, formed by gel-embedded mammary epithelial cells.[85] First, RGD-modified alginate porous scaffolds were produced by combining freeze-drying and particle leaching techniques. Coseeding of human mammary fibroblasts (hMF) and outgrowth endothelial cells (OEC) established the vascular compartment within one week. At this time point, the authors observed OEC alignment, their organization in tubular-like structures, and deposition of ECM proteins (collagen IV and fibronectin) in the scaffolds. Subsequently, epithelial cells suspended in a RGD-modified alginate gel-precursor solution were dispended to the scaffold, forming a hydrogel in situ. After 7 days, epithelial spheroids were detected within the scaffold pores (Figure 3B).

3D hydrogel models can also be employed to investigate the unclear role of cell–matrix interactions in many tumors where dynamic alterations in ECM components are observed. For example, in malignant brain tumors, abnormally high levels of hyaluronic acid (HA) and/or collagen, along with altered expression of many proteoglycans, are associated with disease's development and progression.[86,87] To study these interactions, Sood et al. developed tunable 3D bioengineered platforms by combining microenvironmental cues from native brain-derived ECMs with patient-derived cells from two different tumors: pediatric ependymoma or adult glioblastoma (GBM).[88] Cells dissociated from the excised tumor were seeded in ring-shaped porous silk 3D scaffolds. After one day of incubation, the constructs were infused with collagen type I (CGL1) or HA hydrogels and supplemented with porcine brain-derived ECM. Depending on the infused hydrogel matrix, different cell migration and spheroids formation patterns were observed. In particular, little to no migration of GBM cells was observed within the central window of CLG1-based constructs. In contrast, in HA-infused scaffolds, GMB cells migrated rapidly at early time points and aggregated into multiple spheroids that, within one month, migrated outward from the outer rim of the scaffold. The presence of HA, which is abnormally high in GBM glioblastoma, stimulated patient-derived cells to mimic their in vivo behavior, which could otherwise not be observable with traditional in vitro models.

2.2.2.1. Printed Scaffolds: 3D printing offers significant advantages over previous methodologies for developing in vitro tumor models. It enables the fabrication of high-resolution, precise architectures that can mimic the complexity of the TME.[89,90] This technique allows for the deposition of multiple biomaterials, cells, and biomolecules in a predetermined 3D geometry in a precise and controlled way, through computer-aided designing (CAD). Unlike cancer spheroids, which cannot be formed with

Figure 3. Examples of scaffold-based approaches to develop 3D in vitro cancer models. A) –i) Schematic workflow for the production of electrospun nanofibrous PVA or PVA/Collagen scaffold and cell seeding method. ii) SEM images of A549 cancer cells on PVA/Collagen nanofibrous mat. Cells on the scaffold spread their cytosol and filopodia along the direction of the nanofibers. Scale bars: 10 µm (left and central) and 1 µm (right). iii) RNA expression levels of A549 cells cultured on nanofibrous scaffold with various diameters (90, 170, 220 nm) for 2 days. By qRT-PCR, three multiple markers for EMT were investigated: N-cadherin (N-cad), vimentin (Vim), and fibronectin (Fib). Adapted with permission conveyed through Copyright Clearance Center, Inc.[24] B) –i) Schematic representation of the 3D alginate cancer model development, combining a vascularized stromal with a parenchymal epithelial compartment. ii) CLSM imaging of monocultures of fibroblast and OEC cells after 14 days of culture in RGD-modified alginate porous scaffold, seeded only on top (first two columns) or on both sides of the scaffold (last two columns). Fibroblasts were stained for F-actin (magenta) and fibronectin (FN, cyan). Endothelial cells were stained for laminin (green) and CD31 (red). Scale bar = 200 µm. iii) CLSM imaging after 1 week of tri-culture MCF10A, MCF7, and MDA-MB-231 within the scaffold. Immunostaining for ECM proteins was performed: fibronectin (FN, cyan) and collagen IV (COL IV, yellow). Cell organization is visualized through staining of nuclei (blue) and F-actin cytoskeleton (magenta). Scale bar: 100 µm. Adapted under terms of the CC-BY license.[85] C) – i) Illustration of the printing process to obtain endothelialized liver lobule-like constructs. ii) CLSM imaging of the 3D model at day 1 and day. F-actin (green) and nuclei (blue) were stained to visualize cell morphology and arrangement. Scale bar: 200 µm. iii) Drug testing with Sorafenib on cocultured and mono-cultured liver cancer models at different drug concentrations. Statistical analysis of cell viabilities with $*p < 0.05$ and $**p < 0.01$. Adapted under terms of the CC-BY license.[95]

all cell types and do not fully replicate the tumor microarchitecture, 3D bioprinting has the potential to replicate the TME in its entirety by patterning different biomaterials and cell populations. This results in a biomimetic cancer model that not only replicates the cellular and ECM composition but also maintains the same geometrical arrangement.[91–93] This versatile technique has been used to develop various cancer models for both research and drug development purposes.

For instance, Schmid et al. developed a vascularized melanoma in vitro model, recreating the skin ECM structure using a three-component hydrogel-based bioink composed of 3% gelatin, 0.5% alginate, and 0.1% HA.[94] These biomaterials ware chosen based on skin matrix composition, and their proportions were optimized to ensure both printability and biomimicry. Gelatin, as hydrolyzed collagen, adds thickness to the bioink to achieve the desired construct elasticity and ensures integrin binding. HA facilitates CD44 interaction and significantly impacts angiogenesis and cancer metastasis. Alginate, although not a native skin constituent, was used to tune the ink's stiffness. This bioink maintained the differentiation potential of immortalized adipose-derived mesenchymal cells (ADSCs) into the adipogenic lineage, in contrast to 2D culture substrates, which induce differentiation into the osteogenic line. Malignant metastatic melanoma cells (Mel Im) proliferated in large colonies (over 100 µm in diameters after 14 days) and often escaped the hydrogel construct, consistent with their highly migratory behavior in vivo. This model was tested in vivo in immune-deficient rats with an arteriovenous loop to assess intrinsic vascularization and metastases formation.

An example of the high spatial resolution achievable through 3D bioprinting technique is the realization of a drug screening platform that mimics the liver lobule structure.[95] This model consisted of a three-layer hexagonal structure deposited through dot extrusion printing (DEP) technology, with a hepatocellular carcinoma cell (C3A)-laden Gelatin methacryloyl (GelMA) bioink. To achieve an endothelialized liver cancer model, the authors developed an additional construct depositing 4% gelatin containing HUVECs microbeads on the first hepatocellular carcinoma layer. This layer was sacrificed after GelMA crosslinking to obtain a thin network of endothelial cells fully connected and covering the surface of the primary structure (Figure 3C). GelMa 6% effectively supported C3A cells spheroid growth, with its compression modulus closely matching that of liver tissue and its abundant cell-attachment sites ensuring rapid HUVEC adhesion during the brief sacrificial phase. The biomimetic 3D structure guided endothelial cell extension and network formation. Drug testing with Sorafenib on this endothelialized model demonstrated stronger drug resistance compared to the C3A-only printed construct and 3D spheroids, highlighting the crucial role of endothelium component in the liver TME. This platform may lead to more accurate pharmacodynamic results for in vitro drug testing.

Moreover, 3D bioprinting technique can be employed in precision cancer medicine to help determining the most effective treatment for each patient. A sophisticated GBM glioblastoma model was established to investigate patient-specific drug resistance to conventional treatments using patient-derived cells. The model consisted of a multibioink concentric-ring structure printed on a microfluidic chip.[96] The bioink for the first rings was made from decellularized extracellular matrix derived from porcine brain tissue (BdECM) and was laden with patient-derived cancer cells and vasculature cells (HUVECs) for the inner and outer rings, respectively. An additional outer ring was printed with a gas permeable silicone ink. This structure recapitulates the patient-specific TME in its complexity within a reasonable timeframe of less than 2 weeks. It includes the bio-chemical and mechanical cues of the brain ECM, tumor–stroma interactions anatomically similar to those in native tissue, and the establishment of a radial oxygen gradient simulating the hypoxic core of GBM glioblastoma. The validity of this model was investigated by comparing cell resistance to concomitant radiotherapy and temozolomide treatment (the current standard of care for GBM glioblastoma with 2D cell cultures and 3D spheroids for each of seven patient-derived cells. The glioblastomaGBM-on-a-chip model's responsiveness to treatment diverged from both control populations but better mimicked the clinical response. Overall, the development of 3D cancer models that further mimic in vivo conditions allow scientists to monitor cell behavior thoroughly, focusing on their interactions at the single-cell level and in real-time over extended periods. These analysis techniques will be explored in the subsequent sections.

3. Bulk Versus Single-Cell Analyses

3.1. Limitations of Bulk Analyses

For years, bulk analyses have represented the gold standard for investigating physiological and pathological states, as well for establishing diagnostics, prognostics, and therapeutics schemes. This type of analysis, which relies on microscopy,[97–100] flow cytometry,[101–103] and molecular biology techniques,[104–107] aims to evaluate the cellular and molecular contents of a sample by averaging data collected from a heterogeneous cell population. However, organs are complex environments composed of different tissue microenvironments that orchestrate and regulate physiological functions. Signaling gradients, cell–cell, and cell–ECM extracellular interactions create a multifactorial and intricate network of differential gene expression, resulting in heterogeneity.[108,109] Pathological disorders often disrupt this balance, creating a microenvironment favorable to disease development. Bulk analyses mask the gene expression signatures of subpopulations, as well as changes in proportion and individual activation states, by averaging the entire sample. To address the limitation of bulk analyses, a paradigm shift toward single-cell analyses is necessary. This approach can reveal cell–cell and cell–environment interactions within cancer models that replicate the fundamental features of the TME (**Figure 4**).

3.2. Importance of Single-Cell Analyses

Recent technological advances have provided methods to isolate and identify cells,[110–112] as well as to analyze molecular profiles at single-cell resolution,[113–115] overcoming the limitations bulk analyses.[116,117] While the power of single-cell analyses has been recognized for decades, it is only the advent of simultaneous and integrative multimodal analyses, combined with bioinformatics tools, that has truly begun to reveal the heterogeneous tissue envi-

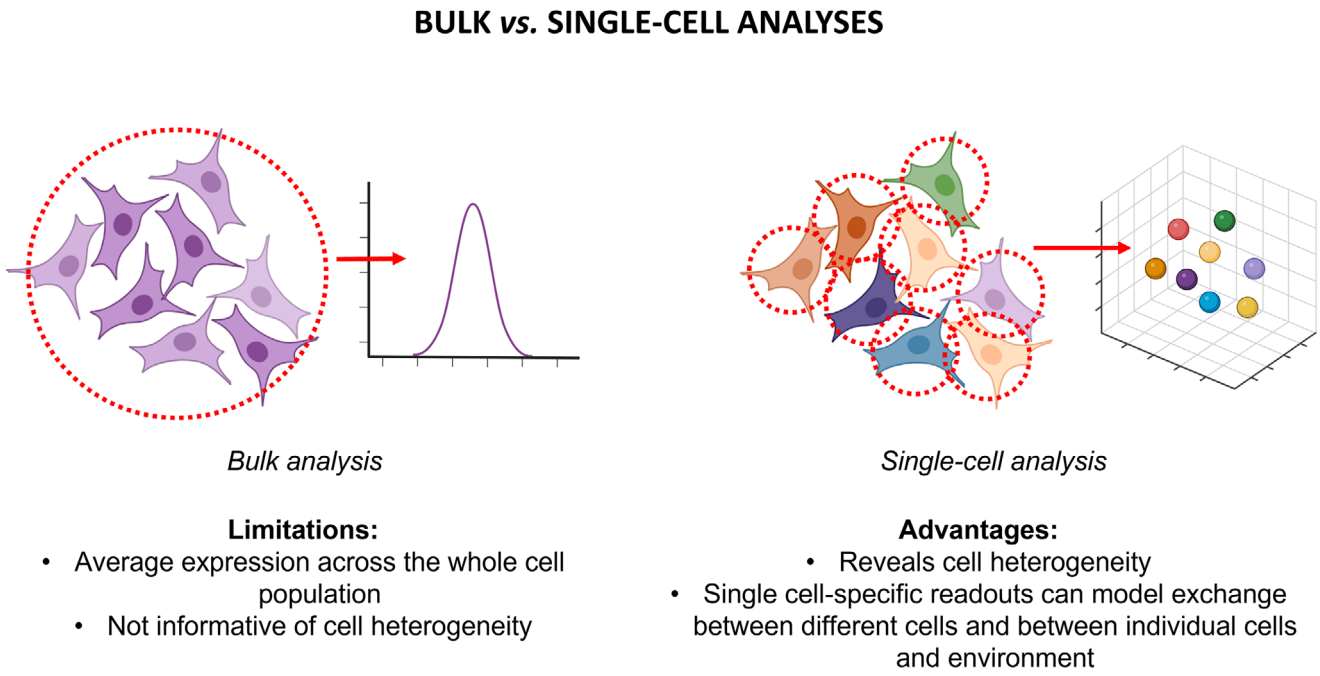

Figure 4. Schematic representation of the main differences between bulk (left) and single-cell (right) analysis of cell populations.

ronment and the interplay between neighbor cells.[118,119] Single-cell genomic, epigenomic, proteomic, and transcriptomic technologies are revolutionizing our understanding of cellular responses and resistance to anticancer treatments.[120,121] In this section, we will discuss recent publications focusing on flow cytometry, microscopy, and multi-omics approaches, as valuable techniques for single-cell analyses.

3.2.1. Flow-cytometry: A Cornerstone for Single-Cell Analysis

Developed in the mid-1970s, flow cytometry is now one of the most advanced and versatile techniques for automated and quantitative analysis of multiple characteristics of individual cells in a high-throughput manner.[122,123] In this approach, cells suspended in an aqueous buffer are hydrodynamically focused to pass in single file through a laser beam, where they are analyzed based on physical parameters or emitted fluorescent light derived from the labeled cells.[124] In combining flow cytometry with fluorescence-activated cell sorting (FACS) allows for the physical isolation of individual cells from heterogeneous populations based on their fluorescence properties for further analyses.[125,126]

In the recent years, flow cytometry has become a cornerstone technique in different research fields, including cell biology, immunology, drug discovery, and oncology.[127] At single-cell level, it has been used to deeply investigate intratumoral heterogeneity. For example, Kieffer et al. identified different subsets of fibroblast CAFs expressing the fibroblast activation protein (FAP) linked to immunosuppression and immunotherapy resistance in breast cancer.[128] By investigating over 19 000 single CAF-S1 cells, the authors identified five clusters characterized by ECM protein expression and signaling pathways related to primary immunotherapy resistance. The discovery of these cluster-specific signatures is crucial for improving new therapeutic strategies in combination with immunotherapies. Similarly, Hutton et al. used single-cell analysis to reveal a fibroblast lineage that supports antitumor immunity in pancreatic ductal adenocarcinoma (PDAC).[129] By analyzing stromal composition in murine tissues and spontaneous tumor models via mass cytometry, they found that CD105-positive fibroblasts allowed tumor growth in vivo, while CD105-negative fibroblasts were highly tumor suppressive, in an adaptive immunity-dependent manner (**Figure 5**A).

Flow cytometry is also employed to characterize the metabolic profile of cancer cells at the single-cell level. Although most metabolic profiling techniques are performed in bulk, Arguello et al. recently proposed a simple method based on flow cytometry to quantify the energy metabolism of various cell types in parallel with single-cell resolution.[130] This technique, named SCENITH (Single Cell ENergetic metabolism by profilIng Translation inHibition) measures protein synthesis levels, which consume a high amount of cellular energy, thus providing a measure of the global metabolic activity. This flow cytometry-based method has been applied to ex vivo metabolic studies in whole blood, lymphoid organs, and myeloid cells in solid tumors, demonstrating its validity for analyzing heterogenous samples.

Overall, flow cytometry single cell analysis provides crucial insights omitted in bulk analyses, improving therapeutic responses and patient stratification.

3.2.2. Advanced Optical Methods for Characterizing Cellular Dynamics in 3D Models

Despite its unquestionable power to unravel tumor heterogeneity, flow cytometry is not able to provide single-cell analyses of intact 3D models. In fact, cells grown in 3D systems need to

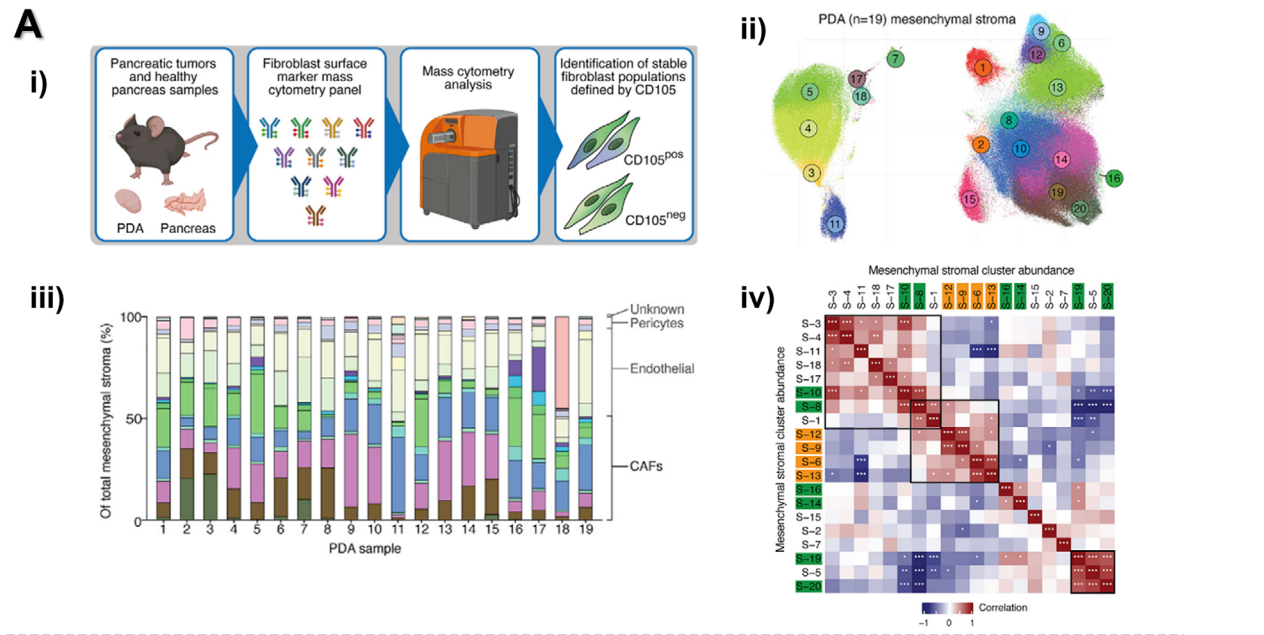

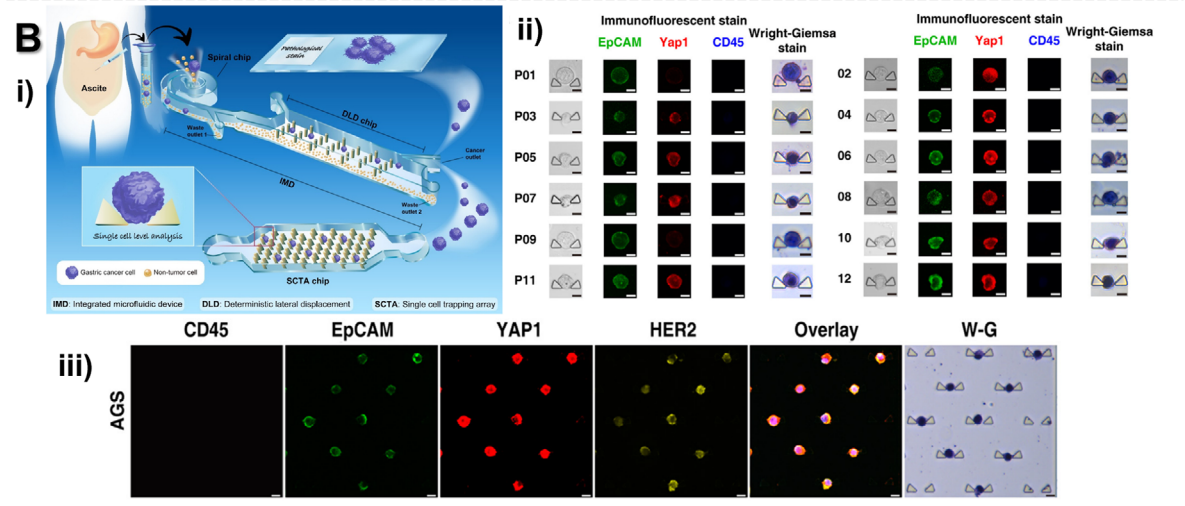

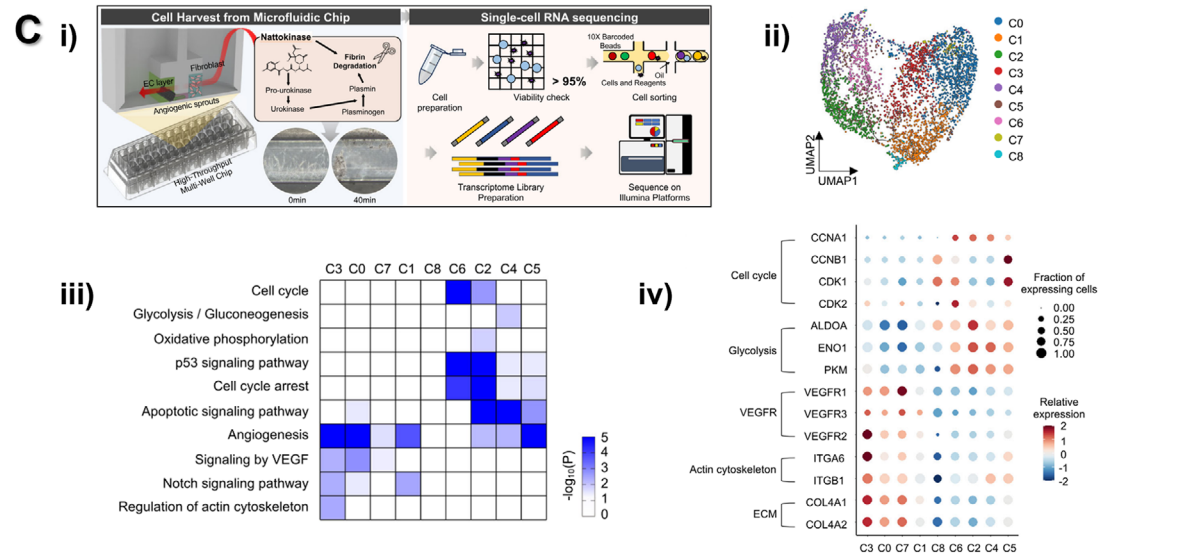

be recovered from their environment before undergoing flow-cytometry. In this context, optical methods could offer a way to characterize cells in 3D models in toto while retaining spatial information.[131] Optical sample sectioning and spatially-resolved approaches can reconstruct intensity profiles as a function of position, granting spatial context for individual cell subpopulations.

Microscopy owns different features that can be suited to characterize cellular models. Firstly, resolution is compatible with subcellular structures. In addition, light sources have a nondestructive nature, and this allows for long-term imaging of living cells in order to measure their dynamics. Notably, since great part of the cell molecules are not fluorescent, a diverse range of fluorescent labels can be introduced enabling proteins, organelles, and other structures to be targeted for imaging, either by genetically encoding fluorescent tags of proteins or by linking fluorescently labeled antibodies.[97,132,133]

Laser scanning confocal (LSC) imaging stands out for imaging intact cell aggregates or entire 3D models with high sensitivity and a good signal-to-noise ratio (SNR). For example, Teixera et al. used confocal microscopy to investigate the role of the stromal component in tumor progression and metastasis in an in vitro 3D model of breast cancer.[85] Confocal imaging visualized cell adhesion within the hydrogel, their organization into tubular-like structures, and heterotypic cell–cell and cell–ECM interactions.

Microfabrication of novel analytical tools able to integrate and precisely manipulate individual cells have been proposed. Microfluidic chips assembled in the shape of cell traps, droplets and microwells have demonstrated to be appropriate tools to investigate cells behavior in the complex TME at a single-cell level through confocal microscopy. Zhao et al. isolated gastric cancer cells from 12 patient ascites samples using a microfluidic single-cell trapping array chip (SCTA chip)[134] and analyzed them using in situ immunofluorescence. This setup allowed the identification of EpCAM+/CD45– cells with intact and hyperchromatic nuclei, and the serial expression analysis of YAP1 and HER-2 via confocal imaging revealed different expression levels according to disease progression (Figure 5B).

Recently, Alieva et al. introduced BEHAV3D, an analytical protocol which exploits multicolor live 3D imaging.[135] The aim of the study was to detect the dynamics of tumor cell death by visualization of individual cell and population, to recognize the behavior of engineered T cells (labeled with fluorescent dyes), and to extract data from 3D images and time-lapse video in order to gain more detailed insights of inter- and intratumor heterogeneity. This protocol was applied to breast cancer, head and neck cancer, and diffuse midline glioma, and allowed to unveil the tumor response to cellular immunotherapy, representing therefore a valid methodology to highlight differences in patients' treatment response.

Multiphoton microscopy (MPM) offers an alternative to LSC microscopy for analyzing thick 3D samples due to its increased penetration depth. This technique is based on near-infrared excitation, thus data acquisition is possible with lower tissue absorption and scattering, hence minimal phototoxicity and low noise SNR.[131]

Kunze et al. used MPM to investigate the collagen-rich ECM remodeling potential of DAPK1 in colorectal cancer.[136] Tumor cells were embedded in an in vivo chorioallantoic membrane (CAM) tissue model and imaged after five days using MPM. This approach allowed the analysis of the invasion front of tumors grown on the CAM in 3D, allowing analysis of the tumor cell–ECM interactions.

Optical methods offer an efficient and rapid strategy for visualizing cell structures, ECM components, and their interactions. However, for a more comprehensive investigation of underlying molecular mechanisms, these methods often need to be combined with other analytical techniques.

3.2.3. Advancements in Multi-Omics for Single-Cell Analysis

Omics sciences, including genomics (DNA), epigenomics (accessible or condensed chromatin), transcriptomics (RNA), and proteomics (protein) analyses, have long been utilized to uncover and examine biomolecular levels in both physiological and disease contexts. Recently, multimodal integrative single-cell omics, incorporating spatial and temporal resolution, are revolutionizing our understanding of normal tissue development, diseases establishment and progression.[137] In particular, cancer, being highly heterogenous in terms of genotypes, phenotypes, and cells states, can benefit from single-cell techniques to recognize the unique features of individual cells. Depending on the tissue origin and its microenvironment, several temporal cellular alterations and responses specific to spatially restricted subpopulations can be linked to immune evasion and tumor progression.

Combining 3D cell culture techniques with multi-omics analyses provides a powerful approach for supporting personalized therapies by characterizing the intricate relationships between genome-associated changes, cellular activation pathways, and protein expression patterns within individual subpopulations in the tumor microenvironment TME. In this context, Lin and collaborators investigated the behavior of osteosarcoma cells in re-

Figure 5. Examples of single-cell analyses. A) –i) Workflow of mass cytometry analysis at level of single-cell of stromal cells in murine normal tissue and in PDAC and their distinction by CD105 expression. ii) UMAP projection of single mesenchymal stromal cells from tumor tissues ($n = 19$) with color-coded FlowSOM clusters (1–20). iii) Relative abundance of KPC PDA mesenchymal stromal subclusters, regrouped into major mesenchymal groups. iv) Spearman correlation coefficients of all pairwise cluster frequencies. CAF subsets CD105-negative (orange) and CD105-positive (green) are highlighted. ns, not significant; $*p < 0.05$, $**p < 0.01$, $***p < 0.001$. Adapted under terms of the CC-BY-NC-ND license.[129] B) –i) Schematic workflow for the separation of gastric cancer cells from ascites by microfluidic techniques and further analysis at the single-cell level in a SCTA-chip. ii) Bright-field, CLSM imaging and Wright–Giemsa staining in the chip for separated cells from 12 patients' ascites. Staining for EpCAM (green), YAP1 (red), and CD45 (blue), were performed. Scale bar: 8 µm. iii) Representative confocal fluorescence images and Wright–Giemsa staining of isolated AGS cells on the SCTA-chip. Immunostaining for CD45 (blue), EpCAM (green), YAP1 (red), HER-2 (yellow), and their overlay are shown. Scale bar: 8 µm. Adapted under terms of the CC-BY-NC-ND license.[134] C) –i) Workflow of scRNA-seq analysis of 3D angiogenic sprouts grown in the microfluidic chip. ii) UMAP plot of ECs with and without Fibroblast condition. Cells are colored by their clusters (C0-C8). iii) Plot of cellular pathways enriched by marker genes of each cluster. Enrichment significance is displayed as –log10(P). iv) Dot plot of the relative expression of marker genes associated with cell cycle, glycolysis, VEGF receptors, actin cytoskeleton, and ECM pathways. Adapted under terms of the CC-BY license.[141]

sponse to antitumor drugs.[138] The authors developed a bioprinted osteosarcoma model embedded in an ECM-like environment, which successfully supported cell viability and proliferation, while facilitating nutrient exchange and drug permeation. Comparative analyses using transcriptomic RNA-seq and DNA methylomics across 2D cultures, spheroids, and the bioprinted model revealed significant differences in the cellular pathways and molecular alterations between these systems. The 3D bioprinted model, combined with comprehensive multi-omics analyses, more accurately reflected cell behavior within a TME-like environment, and helped to identify potential therapeutic targets for chemotherapeutic agents. Tang et al. demonstrated the genotypic and phenotypic heterogeneity of castration-resistant prostate cancer (CRPC) using patients derived organoids (PDOs).[139] Four different molecular subtypes were identified through transposase-accessible chromatin sequencing (ATAC-seq), RNA sequencing (RNA-seq), and DNA sequencing analyses. The authors associated specific transcription factors and gene signatures with each subtype, enabling the separation of CRPC patients accordingly. Target proteins were predicted and validated using transcriptomic data from CRPC patients, highlighting the power of combining in vitro and omics approaches.

In a more refined way, single-cells omics methodologies are invaluable in understanding cellular behavior within the TME. Gong et al. investigated the functional dynamics of immune cells in nasopharyngeal carcinoma (NPC) through integrated research.[140] Single-cell RNA sequencing (scRNA-seq), spatial transcriptome sequencing, and cell–cell interaction analyses allowed to stratify, identify, and functionally classify Treg subpopulation with immunosuppressive activity, recognizing their molecular basis. NPC-derived organoids cocultured with peripheral blood mononuclear cells (PBMCs) were used to validate the data and to predict immunotherapy responses. In a recent work, Lee et al. used an angiogenesis-on-a-chip system to recreate endothelial sprouts and identify endothelial cells heterogeneity.[141] By scRNA-seq analysis, the authors discovered cells exhibiting spatially distinct autophagy activation patterns on the elongating sprouts (Figure 5C). Data analyses from tumoral tissue of breast cancer patients corroborated the findings from the 3D model. Understanding angiogenesis, a hallmark of cancer, is critical for advancing tumor therapeutic strategies.

Recent breakthroughs in single-cell omics analyses, particularly from cancer patients and 3D in vitro models such as immortalized cancer cell lines and patient-derived organoids (PDOs), have started to pave the way for improved clinical management. However, several challenges remain, including the time required to generate complex in vitro tumor models and the need for accurately representing the heterogeneity of the tumor transcriptome landscape. To address these issues, Ding et al. developed a system that rapidly generates patient-derived micro-organospheres (MOS) for drug screening within a clinically relevant timeframe.[142] Their study demonstrated, through single-cell RNA analyses, that the cell populations in MOS closely corresponded to those in patient tumor specimens from various cancers (lung, kidney, ovarian, and colorectal). This platform showed potential for effectively guiding patient treatment decisions. Similarly, Chen et al. used scRNA-seq to study matched PDOs from cholangiocarcinoma and PDAC pancreatic patients alongside their primary tumor samples. Their research revealed both interpatient and intratumoral heterogeneity through transcriptional profiling.[143] Although the organoid composition did not fully replicate the TME and displayed adaptive mechanisms due to culture conditions, the PDOs still exhibited tumor characteristics suitable for drug testing and treatment guidance.

In an interesting study by Tian et al., preclinical, clinical, and translational research revealed mechanisms potentially beneficial for colorectal cancer patients.[144] The authors analyzed paired scRNA-seq data from samples obtained before and during a combinatorial treatment in a phase II clinical trial and simultaneously generated organoids from the same patients. Their matched analyses showed a correlation between signaling pathway inhibition and an enhanced immune response, leading to clinical benefits. This study demonstrated the feasibility of integrating scRNA-seq analyses into treatment regimens to improve clinical outcomes.

However, preparing samples for single-cell analyses remains a challenge in cancer research, particularly with patient-derived fresh samples. Proper logistics and handling are essential to preserve cell viability and membrane integrity, as delays or poor conservation can lead to contamination and low-quality data. Ensuring viable cells and preventing aggregation are critical steps for high-quality single-cell analysis. Coordinated efforts between surgeons and researchers, along with best practices in sample handling, can help mitigate these challenges.[145–148]

Beyond sample preparation, single-cell data analysis presents another hurdle. As methodologies evolve to include integrative multi-analytical spatial and temporal data, the volume of information generated is immense, making it impossible for manual analysis within a reasonable timeframe. Bioinformatics is now indispensable for processing, integrating, and analyzing these datasets. However, the complexity of computational biology, along with the vast array of available tools, poses challenges in selecting the most suitable platform and statistical parameters to extract meaningful insights from the data.[114]

In conclusion, the integration of multi-omics and single-cell analyses is proving essential for unraveling the heterogeneity of tumors and identifying new therapeutic targets for cancer patients. Nonetheless, clinical applications, such as decision-making treatment strategies based on these combined approaches, remain a work in progress and require further refinement. Additionally, incorporating time-resolved omics methods is crucial for advancing cancer research, as we will discuss in the following sections.

4. Endpoint Versus Live-Cell Analyses

4.1. Limitations of Endpoint Analyses

The gold standard for investigating tumor progression has traditionally been endpoint analyses, allowing for long-term studies of cellular behavior. This method involves examining data at specific intervals during cell development, treatment, and follow-up.[149,150] Researchers track changes in cell characteristics, biomarker expression, therapeutic responses, and cellular progression by capturing snapshots of cell development.

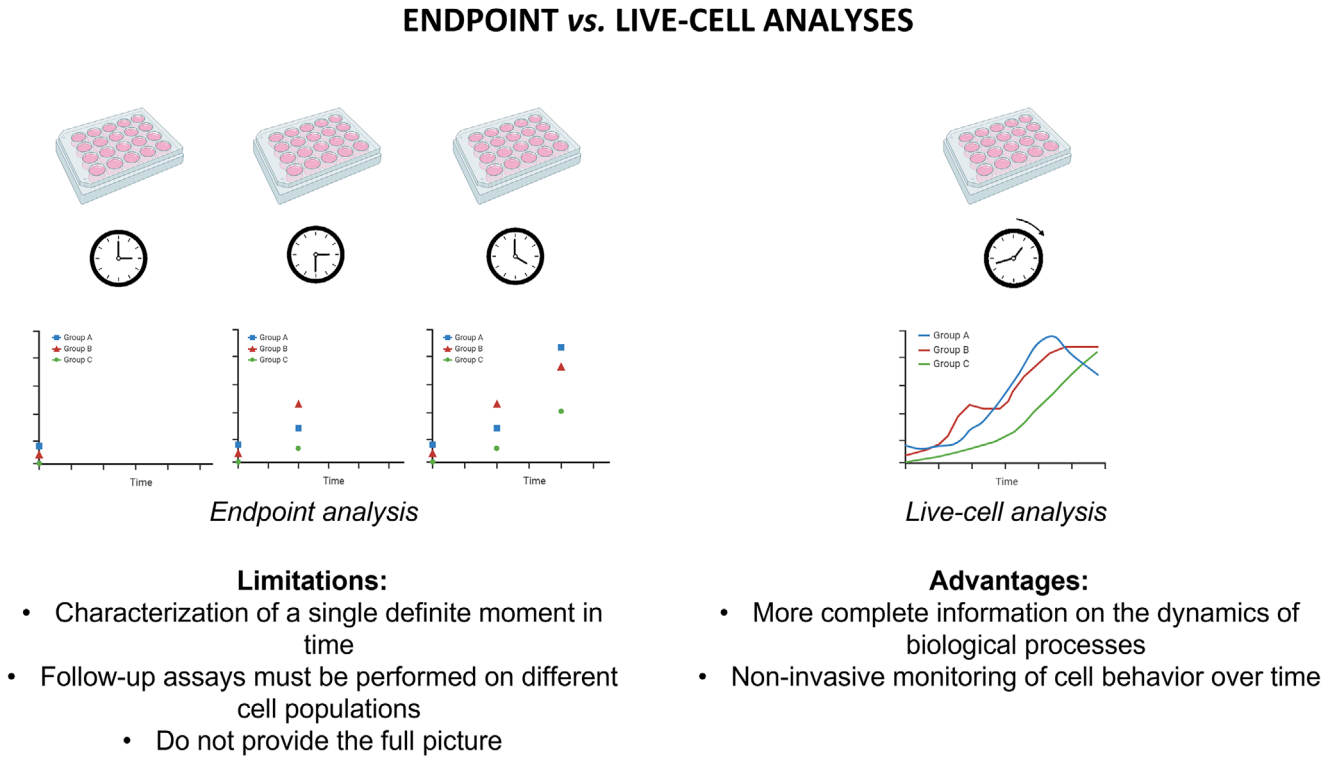

Figure 6. Schematic representation of the main differences between endpoint (left) and live-cell (right) analysis.

These snapshots help to identify critical milestones, elucidate underlying mechanisms, and develop new therapeutic strategies. However, endpoint analysis has inherent limitations affecting its interpretive power and clinical relevance (**Figure 6**).[151] One major challenge lies in its reductionism, particularly in cancer research. Endpoint analyses simplify cancer complexity by isolating moments in the disease process,[152] overlooking continuous tumor evolution, missing nuances of intratumoral heterogeneity, clonal dynamics, and microenvironmental influences.[153] Such oversimplification can lead to missed subtle but clinically significant changes over time. Additionally, endpoint analysis is constrained by the frequency and timing of data collection.[154] Cancer progression is nonlinear, with periods of rapid growth, dormancy, and metastasis.[15] Traditional endpoint intervals, such as post-treatment check, may miss crucial transitional phases and emergent phenomena, hiding critical events and impeding predictive modeling. Furthermore, endpoint analysis offers a static view of disease progression and cellular response. Cancer is a dynamic system influenced by an array of intrinsic and extrinsic factors, including genetic mutations, epigenetic modifications, immune surveillance, and therapeutic interventions.[155,156] Endpoint analysis often fails to capture the temporal dynamics of these factors, treating each observation as independent and static. This approach may underestimate tumor evolution complexity, treatment resistance mechanisms, and adaptive responses, limiting the predictive accuracy of temporal models and therapeutic strategies. Consequently, rare events, such as the transition from solid tumor cell to circulating tumor cells that can be missed without the proper tracking.

4.2. Importance of Live-Cell Analyses

Live-cell analysis enables the study of cellular dynamics in real time, offering a more comprehensive view compared to static snapshots of single time points. This noninvasive monitoring allows to follow cell arrangement and modification during disease progression, providing a clearer picture of the dynamic and heterogeneous microenvironment. Cancer cells, unlike healthy tissues, lack rigorous cell cycle control, giving them an advantage in f growth and proliferation. In this scenario, morphometric dynamics help identify specific cellular states, new mechanisms of cellular signaling modulation, and novel cell populations, otherwise hardly noticeable with static methodologies.[4,157] Moreover, live-cell analyses are crucial for understanding the dynamic responses of tumors to treatment, capturing cellular and signaling events in real time. This approach has the potential to identify biomarkers that could enhance therapeutic efficacy and enhance clinical outcomes.[158–160] In the following sections, we will discuss different techniques for continuous analysis in oncology research, including the Seahorse analyzer, optical metabolic imaging OMI, live imaging microscopy, and Raman spectroscopy. These methods provide invaluable insights into the complex behavior of cancer cells, paving the way for more effective treatments.

4.2.1. Real-Time Cell Metabolic Analyzer

Cellular metabolism involves the uptake of substrates such as oxygen, glucose, and fatty acids, and their conversion into en-

ergy through enzymatically controlled oxidation/reduction reactions. These reactions occur via intracellular biochemical processes including glycolysis, Krebs cycle, electron transport and oxidative phosphorylation (OXPHOS), resulting in ATP production and the release of heat and chemical by-products like lactate and CO_2 into the extracellular environment.[161] Monitoring the metabolic states of cells within complex microenvironment, such as the TME, and their dynamic responses to physiological stimuli is crucial. Evaluating the metabolic state of a statistically significant sample alone is insufficient for the aforementioned purposes.

Kinetics studies of biological parameters such as pH, oxygen, potassium, lactate, and glucose allow to evaluate mitochondrial function, cellular glycolysis, bioenergetic profiles, and oxidative stress in various diseases.[162–165] These studies also track metabolic fluxes in cancer models (e.g., spheroids)[166] and identify metabolic phenotype switches (e.g., in T cells and in cancer cells),[165] evaluating cell oxygen consumption and extracellular acidification.[167] These parameters are typically monitored using spectrofluorimetric techniques, which measure variations in fluorescence intensities displayed by optical probes interacting with different concentration of the target analyte over time. The Agilent Seahorse Analyzer (Agilent), along with the Seahorse Cell Mito Stress Test kit, is a widely used spectrofluorimetric methodology and is considered the gold standard for measuring cellular metabolic activity in bulk. This fully integrated multiwell instrument evaluates the extracellular fluxes (XF) and the uptake/excretion of metabolic end products of adherent cells in a microplate over time, enabling rapid, real-time detection of metabolic changes. Specifically, it measures changes in mitochondrial metabolism and cellular respiration or glycolysis rates due to experimental manipulation.[168–170] The instrument quantifies the oxygen consumption rate (OCR) and extracellular acidification rate (ECAR), providing average concentration changes of analytes over in time. The Seahorse methodology has been utilized to identify and track metabolic phenotype switches in cancer cells. Wu et al. performed a detailed bioenergetic analysis of H460 and A549, two human lung cancer cell lines.[161] They evaluated the metabolic responses of these cell lines to pharmacological modulators of oxidative and glycolytic energy metabolism, simultaneously recording OCR and ECAR. The study revealed distinct bioenergetic phenotypes characterized by high glycolysis rates and attenuated mitochondrial respiration capacity, with H460 cells displaying a more glycolytic behavior and greater impairment of mitochondrial respiration compared to A549 cells. Somova et al. developed an in vitro renal cell carcinoma (RCC) that mimicked the interplay between healthy and malignant renal tissue combining healthy renal proximal tubule epithelial cells (RPTEC) and RCC cells.[171] Metabolic analysis of cocultured RPTEC tubules and RCC spheroids in a closed micro-perfused circuit showed significant phenotypical changes in the tubules. Seahorse measurements indicated that RCC induced a shift in the energy production of RPTEC tubules toward glycolysis, likely supporting RCC growth and immunogenicity. RCC cells, however, maintained stable metabolic activity, emphasizing their resilience to external factors (**Figure** 7A).

In a different approach, Hunt et al. demonstrated how the solid TME imposes a compromised metabolic state on tumor-infiltrating T cells (TILs), marked by an inability to maintain effective energy synthesis for antitumor function and survival.[172] In order to overcome nutrient stress, T cells in the TME must catabolize lipids via mitochondrial fatty acid oxidation (FAO). T cells enriched in FAO are adept at cancer control. The study revealed that the TME imposes perpetual acetyl-coenzyme A (CoA) carboxylase (ACC) activity, invoking lipid biogenesis and storage in TILs, which opposes FAO. Using Seahorse metabolic analysis, the authors found that restricting ACC activity rewired T cell metabolism, enabling energy maintenance under TME stress, sustaining T cell longevity and functionality, enhancing cancer control.

Despite its reliability, the Seahorse technology is primarily restricted to simple cell cultures, such as adherent monolayers or cells suspensions, and its application to 3D models is still poorly optimized and limited to spheroids.

To improve the investigation of real-time changes in cell metabolic activity at level of single cell, optical metabolic imaging (OMI) has been developed. OMI is a noninvasive, fast, and high-resolution approach to monitor cellular metabolism by detecting and quantifying autofluorescent activity already present in the cells from co-enzymes reduced nicotinamide adenine dinucleotide (NADH) and flavin adenine dinucleotide (FAD).[173–176] Different studies relied on this methodology to evaluate the dynamic and heterogeneous drug response at single-cell level in patient-derived pancreatic cancer organoids[177] and in breast cancer cell lines.[178] Cannon et al. used OMI to quantify dynamic cell-level metabolic differences in drug response between 2D cell lines and 3D organoids generated from breast tumors, proving that this technique is sensitive enough to provide insight on dynamic changes in the relative abundance of metabolic cell subpopulations that contribute to drug resistance in 3D cancer in vitro models.[179]

4.2.2. Live-Cell Imaging: Advancing Understanding of Cellular Dynamics in Real-Time

As previously introduced, cell imaging microscopy plays a crucial role in various scientific disciplines, including cell biology, medicine, pharmacology, and microbiology, as it allows the visualization and analysis of the structure, function, and behavior of individual cells or groups of cells in their natural environment or in vitro.

Endpoint cell imaging has been widely used to visualize and analyze cells after treatment or experimental manipulation at a specific time point after having typically fixed and stained them with fluorescent probes. Several are the applications, including the visualization of subcellular structures (e.g., nucleus, cytoskeleton, mitochondria, and endoplasmic reticulum), studying protein localization and distribution within cells, examining cellular processes such as cell cycle progression, apoptosis, and autophagy,[180,181] analyzing biomolecular interactions and signaling pathways, and investigating changes in cellular morphology and structure in response to experimental conditions or treatments.[182–184] Overall, endpoint fluorescent imaging provides valuable insights into the structure, function, and behavior of cells and their components at a specific time point, contributing to the understanding of cellular biology and various biological processes.

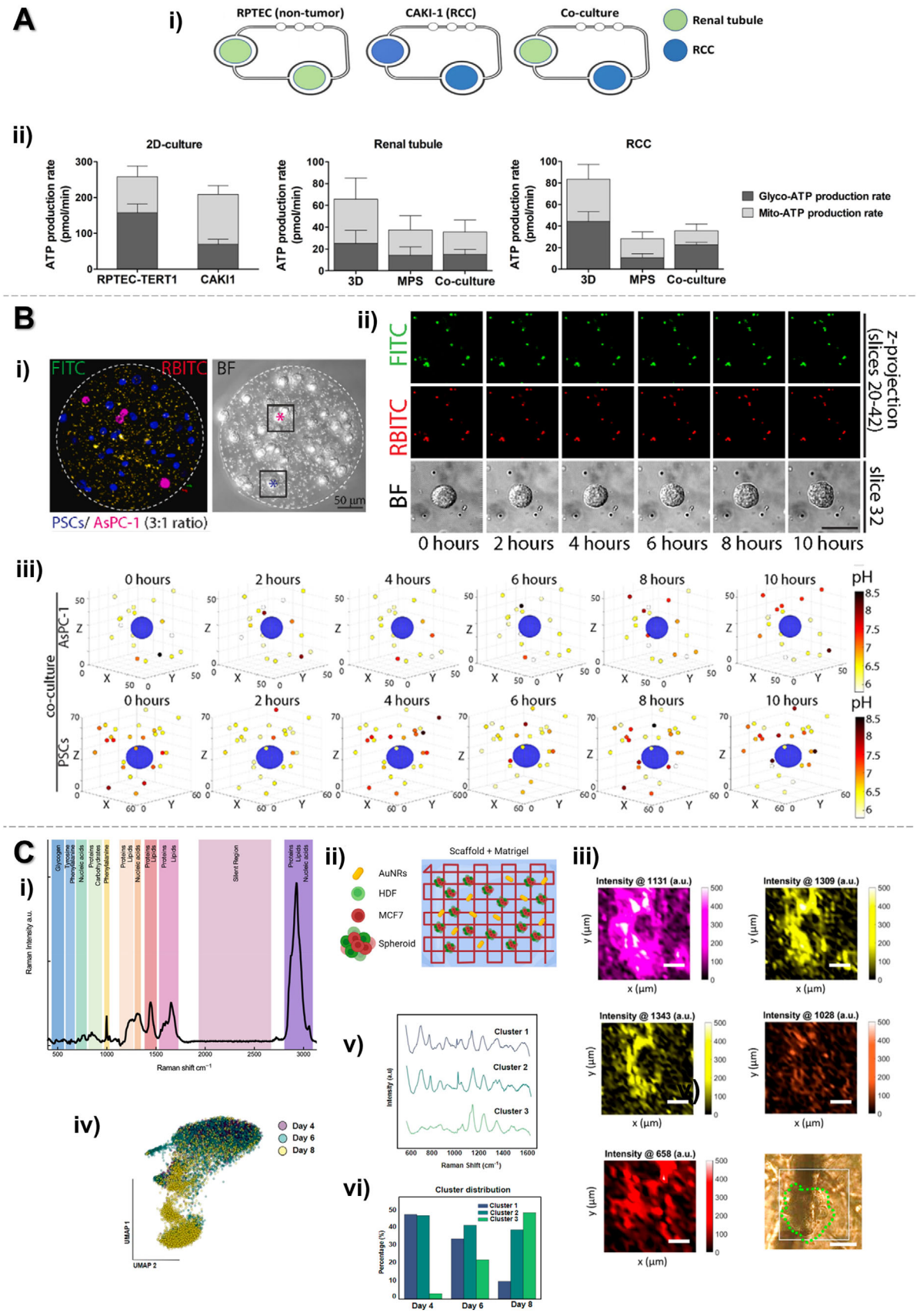

Live-cell imaging, however, provides a more comprehensive view by maintaining cell viability and growth during imaging, ensuring precise and stable incubator conditions (temperature, humidity, CO_2 levels, O_2 eventually) on the microscope. In comparison to single snapshots taken at specific time points, live-cell imaging allows for the continuous observation of cellular dynamics, such as growth and development, over time, and helps identify suitable time points for endpoint investigations, which can be challenging to determine accurately.

For example, live-cell imaging has been used as additional technique to evaluate the efficacy of anticancer therapeutic drugs and drug repurposing by optimizing cell growth conditions and endpoint times for viability assays in various human prostate cancer cell lines.[185] Similarly, Xing et al. used time-lapse imaging and MTT endpoint assays to predict the efficacy of chemotherapy on breast and colon tumor slices embedded in agarose, demonstrating the utility of 3D tumor slice platforms for anticancer drug discovery.[186]

Live-cell imaging also enables real-time the monitoring of cell-death phenomena, providing significant indications of disease conditions and therapy effectiveness. Vicar et al. observed time-lapse morphological changes in prostate cancer cell mass distributions such as the "dance of death", swelling and membrane rupture.[187]

Tracking cell migration, self-organization, or invasion over time is crucial for understanding processes like embryonic development, tissue repair or cancerous tissues growth. Long-term time-lapse investigations of mammary epithelial cell spheroid formation and growth have provided insights into initial breast cancer invasion into a collagen-rich ECM, reproducing a 3D model of cell–cell and cell–matrix interactions.[188] Live confocal imaging has also allowed the observation of glandular branched tissues morphogenesis, where organoids from primary pancreatic PDAC cells in collagen self-organized to reproduce the in vivo PDAC architecture, revealing specific phases of organoid morphogenesis characterized by unique patterns of cell proliferation, invasion, matrix deformation and protein expression.[189]

Live-cell imaging is widely used to capture the complex intricacies of cellular dynamics and cell–cell interactions, which are crucial for organism survival. Fluorescent time-lapse microscopy of tumor–stroma cocultures during chemotherapy has effectively quantified the heterogeneity of drug response in cancer-stroma kinetics.[190] In this study, an extremely fast and cheap computational approach was developed, utilizing only time-lapse fluorescence microscopy to precisely quantify cell–cell interactions and their effects on cellular dynamics. This method computed interactions among pancreatic stroma cells and pancreatic cancer cells, revealing variations in cancer-stroma kinetics and quantifying heterogeneity in drug response in an in vitro coculture model. The proposed approach can also monitor cell kinetics under different cellular perturbations, representing a powerful tool with broad applications in computational biology.

Recently, time-lapse microscopy has shown potential also for recording metabolic changes in complex 3D cocultures with high temporal resolution and at the single-cell level. Mono- and cocultures of tumor and stromal pancreatic cells were embedded into 3D spherical alginate microgels and pH metabolic variations were monitored and quantified over time. This revealed differences in the metabolic crosstalk of tumor and stromal cells (Figure 7B).[191]

After image acquisition, time-lapse image sequences can be analyzed with specialized algorithms to precisely quantify cellular dynamics over time. These analyses include quantifying cell tracking, measuring cell migration and proliferation, changes in cell morphology, and analyzing cellular events such as division, apoptosis, or intracellular trafficking.[192–197] However, quantifying parameters from single cells in spatio-temporal motion remains challenging due to various variables, such as vibrations, illumination, cell motility, focus maintenance, pH, temperature and humidity fluctuations, which may interfere with the acquisition of high-quality images.[198,199] Additionally, repeated fluorescence excitation can cause phototoxicity, affecting the cell cycle, cell divisions, and increasing cell death during imaging.[198,200] Solutions include reducing laser intensities and exposure times, and increasing the length of image acquisition intervals. While this reduces phototoxicity, it must be balanced with the detection times of cellular transitions or biological phenomena and the tracking of cell positions to ensure accurate image acquisition and analyses.

Another approach for real-time monitoring of cellular dynamics using fluorescent microscopy involves fluorescence lifetime imaging microscopy (FLIM) measurements. Unlike intensity-based imaging, FLIM is independent of excitation intensity fluctuations, sample thickness, and photobleaching.[201] FLIM has been widely used for monitoring oxidation-reduction chemistry in real-time, which is crucial for extensively understanding of cell

Figure 7. Examples of live-cell analyses. A) – i) Illustration of the experimental set-up for the metabolic analyses in a microfluidic RCC in vitro model, comprising two connected compartments to simulate the circulation between cancer and healthy epithelium in the renal tubule. Three different conditions were investigated: RPTEC tubules in monoculture (left), RCC spheroids in mono-culture (central), and coculture of RPTEC tubules and RCC spheroids (right). (ii) Metabolic activity analysis based on OCR and ECAR by Seahorse Analyzer. ATP production rate was measured in traditional 2D-cultures for both monocultures (RPTEC-TERT1 and CAKI1 cells) (left), in renal tubules (central), and in RCC spheroids (right). Energy produced by glycolytic metabolism (dark gray) and mitochondrial respiration (light grey) could be distinguished. Adapted under terms of the CC-BY license.[171] B) –i) Representative CLSM imaging of an alginate hydrogel incapsulating pancreatic tumor cells (AsPC-1, magenta), stromal cells (PSC, blue), and FITC/RBITC pH sensors (yellow) and correspondent bright-field (BF) image. Scale bar: 50 µm. ii) Maximum intensity z-projection of the ratiometric fluorescent pH sensors surrounding a single cell. Green channel: sensitive dye (FITC), red channel: reference dye (RBITC), and bright-field (BF). iii) 3D mapping of sensors surrounding a cell over time with relative pH colormap. Adapted under terms of the CC-BY license.[191] C) – i) Raman spectrum of a single cell of human glioblastoma (U87), with the various bands representative of cellular constituents. Adapted from Xu et al. under terms of the CC-BY license.[216] ii) Schematic representation of the scaffold for the SERS biosensing of spheroids made of MCF7 and HDF cells in presence of ligand-free AuNRs as SERS enhancers. iii) Representative SERS peak intensity maps for the Raman peaks identified by Principal Component Analysis (PCA) around a single spheroid (green dashed line in the optical image, bottom right) at day 4 of culture. Scale bar: 50 µm. iv) UMAP of the whole spectra collected at 4, 6, and 8 days of culture showing vibrational changes are mainly related to progression over time. v) SERS average spectra for each clusters identified in (iv). vi) Percentual distribution of spectra across the three clusters at 4, 6, and 8 days of culture. Adapted under terms of the CC-BY-NC-ND license.[226]

metabolism in healthy and pathological conditions. For example, intrinsic NADH fluorescence was acquired with FLIM to examine its metabolic states in the TME either in vitro or in orthotopic mouse xenograft models of GBM, showing that NADH lifetimes were longer for all tumor tissues compared to the healthy ones, and directly correlating the contribution of bound NADH with decreased survival.[202] Shirmanova et al. employed multiparametric FLIM in time-lapse to explore the relationships between the redox status and reactive oxygen species (ROS) in colorectal cancer cells, important regulators of apoptosis. Their aim was to overcome apoptotic resistance during drug treatments.[203] Differently, based on photon counts of FLIM, it is also possible to quantify G-quadruplex DNA in in situ live cells by using a tripodal cationic fluorescent probe (NBTE). Differences in the G-quadruplex DNA level can have important insights in cancer cell detection, indeed, the authors measured a G-quadruplex DNA amount fourfold greater in cancer cells than in normal cells.[204]

With the aim of increasing imaging penetration depth (i.e., spatial resolution) and lifetime measurement accuracy also two-photon or multiphoton FLIM technologies have attracted attention in cancer research.[205] Various biomedical applications of two-photon FLIM have been reviewed, as for example noninvasive clinical diagnostic tool of digestive tract tumor.[206,207] Recently, multiphoton FLIM was used to investigate over time the fluorescence lifetime of endogenous fluorophores in 3D breast cancer spheroids derived from cell lines embedded in collagen with varying densities, evidencing the presence of spatial-metabolic gradients and in particular a shift toward oxidative phosphorylation of the cells of the spheroids in contact with the collagen matrix and of the ones that migrated the farthest.[181] Furthermore, multiphoton FLIM found successful application in vivo from the development of multiphoton tomography which uses tissues autofluorescence and a near infrared femtosecond laser to provide a fast and noninvasive measure with picoseconds temporal resolution.[208]

4.2.3. Raman Spectroscopy: A Powerful Tool for Live-Cell Analyses

Raman spectroscopy, first described nearly 100 years ago as a new methodology[209], has since been used to elucidate the physicochemical properties of many materials.[210] More recently, it has emerged as a powerful and versatile tool in cell biology, offering unique insights into cellular dynamics under physiological conditions.[211,212]

Raman spectroscopy plays a crucial role in cell biology by enabling the detailed characterization of cellular components. By analyzing the Raman spectra of biological samples, researchers can identify and quantify various biomolecules such as proteins, lipids, nucleic acids, and carbohydrates (Figure 7C,i).[213–216] This information is crucial for understanding cellular biochemical processes and their responses to external influences. Moreover, Raman spectroscopy offers insights into dynamic cellular processes, such as metabolic activities, protein folding, and cell signaling. By monitoring changes in Raman spectra over time, researchers can gain valuable information about cellular function and response to stimuli. This capability has significant implications for biomedical research, drug discovery, and disease diagnosis.[217]

Recent studies demonstrate the application of Raman spectroscopy in analyzing breast cancer cell line, revealing that MCF-7 cells exhibit specific modes such as amide I at 1656 cm^{-1}; amide III at 1242 cm^{-1}; a combination of lipids and proteins at 855, 1257, 1300, 1338, and 1447 cm^{-1}; nucleic acid as DNA in 782 cm^{-1}. Notably, this spectrum showed lower intensity in cells with vacuoles, averaging half the intensity observed in other cells.[218] Another study mapped subcellular enrichment of glycogen in HELA cells using Raman scattering, identifying distinct glycogen metabolic phenotypes. After validation, melanoma cells with BRAF mutations displayed a high glycogen-accumulation phenotype and significant resistance to glucose deficiency.[219]

Combining Raman spectroscopy with Fourier transform–infrared (FT-IR) spectroscopy provides complementary information for understanding the structure, function, and biochemical changes in fixed or live cells, even with spatial resolution. Analyses, of MIA PaCa-2 and MDA-MB-231 cell lines (pancreatic and breast cancer, respectively) showed increased bands associated with nonpolar groups (C–H vibrations 3050–2800, ≈1446 cm^{-1}, and ≈1330 cm^{-1}) in fixed cells, while bands associated with polar groups (N–H stretch at ≈3300 cm^{-1} and amide I at 1656 cm^{-1}) were increased. In live cells, Raman spectra from 1743 to 912 cm^{-1} revealed a strong band at 1660 cm^{-1} related to amide I, with the amide II band being much weaker compared to infrared analysis. The most prominent band in the analyzed region was 1446 cm^{-1} related to δCH_2. Additionally, bands between 1340 and 1240 cm^{-1} represented vibrations of amide III, consistent deformations of N-H and C-H, while the symmetric PO_2 stretch at 1237 cm^{-1} was primarily from DNA and RNA, as evidenced by its significantly higher signal in the nucleus.[220,221] The presence of water in live cells can pose challenges for lower spectra readings due to its high peaks at 3250 cm^{-1} and 3470 cm^{-1},[222] but does not interfere with biologically significant peaks below 3100 cm^{-1}, such as amide I and amide II (≈1650 cm^{-1} and ≈1550 cm^{-1}, respectively).[223]

Due to its label-free and nondestructive nature, Raman imaging can be used to noninvasively image cancer cells and study the internalization kinetics and localization of anticancer therapy agents. For example, a recent study by Annušová et al. tracked molybdenum bioconjugate nanoparticles (with peaks at ≈350 cm^{-1} and ≈730 cm^{-1}) in cervical squamous carcinoma cells using label-free live cell confocal Raman microscopy. The study demonstrated preferentially internalization of these nanoparticles in lysosome-rich regions of cancer cells expressing carbonic anhydrase IX (CAIX), a hypoxia marker associated with poor prognosis tumors, as confirmed through flow cytometry and fluorescence microscopy.[224] Active targeting observable through Raman microscopy can streamline nanoparticle delivery and therapeutic success, enabling live monitoring the entire process. Nanotags can facilitate high-resolution time-lapse live-cell Raman imaging. Gu and colleagues developed ultrabright gap enhanced resonance Raman tags (GERRTs) consisting of a petal-like gold core and silver shell with near-infrared resonant reporters. Upon 785 nm excitation, the authors successfully tracked living HeLa cells for extended periods with minimal photodamage, capturing dynamic cellular processes with high temporal resolution and speed (1 ms per pixel).[225]

In a recent work, García-Astrain et al. developed a 3D printed hydrogel platform integrating biosensing and imaging of 3D

breast cancer cell models in situ through surface-enhanced Raman scattering (SERS).[226] The researchers created a polyethylene glycol diacrylate (PEGDA) 3D-printed scaffold incorporating ligand-free gold nanorods (AuNRs) for sensing of cell-secreted metabolites and SERS-labeled nanoparticles for 3D imaging. This construct allowed monitoring of morphological changes in MCF7 and HDF heterotypic spheroids and analyzing spatiotemporal profiles of secreted molecules for up to 21 days, revealing that these tumoroids physically and biologically remodel their ECM according to cancer cell plasticity (Figure 7C,ii–vi).

5. Conclusions

Over the years, the importance of 3D in vitro models has become increasingly evident. A growing number of studies have benefited from tunable platforms that offer greater control over mimicking the TME, ultimately aiming to "replace, reduce, and refine" animal use in experimental protocols.

In this review, we summarized the state-of-the-art of 3D cancer models, highlighting the most outstanding techniques for their development and showcasing some intriguing applications. These examples demonstrate that shifting from 2D cell cultures to 3D models is essential for a deeper understanding of cancer hallmarks. Unfortunately, the use of effective 3D platforms in cancer research is still limited by issues of reproducibility and standardization of procedures. Critical insights from existing studies can help develop models that more closely resemble in vivo tumors. These improved models can be adapted for clinical use, aiding scientists in developing personalized medicine and oncologists in enhancing cancer patient care.

In addition to developing robust models, the availability of appropriate technologies for real-time monitoring of cells at single-cell resolution is crucial for the progression of cancer research. We discussed the emerging need to improve analysis methods for investigating these 3D cell models at the single-cell level, especially through microscopy and multi-omics techniques. These advancements will enable researchers to account for cell heterogeneity, cell–cell and cell–ECM interactions while retaining spatial resolution of the analysis. A further step toward a deeper understanding of the TME involves combining this type of analysis with live cell studies. We showed that cancer progression is a complex, dynamic process that shall not be fully investigable only with traditional time-point assays but requires continuous monitoring. The advent of innovative microscopy and spectroscopy procedures could represent a turning point in live-cell monitoring, allowing scientists to inquire the TME evolution over time. This approach offers a comprehensive and detailed view of cellular dynamics in response to drug treatments, reducing variability and enabling the monitoring of long-term effects.

Altogether, these 3D systems and advanced analytical conditions will open new perspectives for in vitro screening of cellular and molecular determinants of cancer development and progression.

Acknowledgements

This work was supported by the European Research Council (ERC) under the European Union's Horizon 2020 Research and Innovation Program ERC Starting Grant "INTERCELLMED" (n. 759959), the Associazione Italiana per la Ricerca contro il Cancro (AIRC) (MFAG-2019, n. 22902), CAPES (Finance code 001, CAPES/PrInt 2598/2018 processes 88881.311846/2018-01, 88887.311846/2018-00, 88887.311851/2018-00), CNPq for PhD fellowship, the "Tecnopolo per la medicina di precisione" (TecnoMed Puglia) – Regione Puglia, n. B84I18000540002), the Italian Ministry of Research (MUR) in the framework of the National Recovery and Resilience Plan (NRRP), "NFFA-DI" Grant (B53C22004310006), "I-PHOQS" Grant (B53C22001750006) and "Fit4MedRob" Grant (PNC0000007, B53C22006960001) under the complementary actions to the NRRP funded by NextGenerationEU, the PRIN 2022 (2022CRFNCP_PE11_PRIN2022) and the PNRR-MCNT2-2023-12377885 funded by the European Union – Next Generation EU, M6/C2_CALL 2023 (F53C23001360008, B53C23008470005).

Open access publishing facilitated by Consiglio Nazionale delle Ricerche, as part of the Wiley - CRUI-CARE agreement.

Conflict of Interest

The authors declare no conflict of interest.

Keywords

3D models, cancer, live-cell analyses, single-cell analyses, tumor microenvironment

Received: August 9, 2024
Revised: October 23, 2024
Published online:

[1] B. F. Ferlay, J. Ervik, M. Lam, F. Laversanne, M. Colombet, M. Mery, L. Piñeros, M. Znaor, A. Soerjomataram, I. Lyon, France: International Agency for Research on Cancer. **2024**. https://gco.iarc.who.int/today
[2] H. Maeda, M. Khatami, *Clin. Transl. Med.* **2018**, *7*, 1.
[3] *Nature* **2022**, *601*, 297.
[4] L. F. Lorenzo-Martín, T. Hübscher, A. D. Bowler, N. Broguiere, J. Langer, L. Tillard, M. Nikolaev, F. Radtke, M. P. Lutolf, *Nature* **2024**, *629*, 450.
[5] N. Riggi, F. de Sousa e Melo, *Nature* **2024**, *629*, 292.
[6] W. Li, Z. Zhou, X. Zhou, B. L. Khoo, R. Gunawan, Y. R. Chin, L. Zhang, C. Yi, X. Guan, M. Yang, *Adv. Healthcare Mater.* **2023**, *12*, 2202609.
[7] R. J. Seager, C. Hajal, F. Spill, R. D. Kamm, M. H. Zaman, *Converg. Sci. Phys. Oncol.* **2017**, *3*, 034002.
[8] Y. Li, X. Hu, R. Lin, G. Zhou, L. Zhao, D. Zhao, Y. Zhang, W. Li, Y. Zhang, P. Ma, H.u Ren, X. Liao, P. Niu, T. Wang, X. Zhang, W. Wang, R. Gao, Q. Li, G. Church, J. He, Y. Chen, *Theranostics* **2022**, *12*, 3818.
[9] K. Baghy, A. Ladányi, A. Reszegi, I. Kovalszky, *Int. J. Mol. Sci.* **2023**, *24*, 17536.
[10] N. K. Karamanos, A. D. Theocharis, Z. Piperigkou, D. Manou, A. Passi, S. S. Skandalis, D. H. Vynios, V. Orian-Rousseau, S. Ricard-Blum, C. E. H. Schmelzer, L. Duca, M. Durbeej, N. A. Afratis, L. Troeberg, M. Franchi, V. Masola, M. Onisto, *FEBS J.* **2021**, *288*, 6850.
[11] A. Padhi, A. S. Nain, *Ann. Biomed. Eng.* **2020**, *48*, 1071.
[12] D. B. Flies, S. Langermann, C. Jensen, M. A. Karsdal, N. Willumsen, *Front. Immunol.* **2023**, *14*, 1199513.
[13] C. Bonnans, J. Chou, Z. Werb, *Nat. Rev. Mol. Cell Biol.* **2014**, *15*, 786.
[14] M. Wang, J. Zhao, L. Zhang, F. Wei, Y.u Lian, Y. Wu, Z. Gong, S. Zhang, J. Zhou, K.e Cao, X. Li, W. Xiong, G. Li, Z. Zeng, C. Guo, *J. Cancer* **2017**, *8*, 761.
[15] F. Francescangeli, M. L. De Angelis, R. Rossi, A. Cuccu, A. Giuliani, R. De Maria, A. Zeuner, *Cancer Metastasis Rev.* **2023**, *42*, 197.

[16] Q. Wang, X. Shao, Y. Zhang, M. Zhu, F. X. C. Wang, J. Mu, J. Li, H. Yao, K. Chen, *Cancer Med.* **2023**, *12*, 11149.
[17] H. A. Goubran, R. R. Kotb, J. Stakiw, M. E. Emara, T. Burnouf, *Cancer Growth Metastasis* **2014**, *7*, 92.
[18] C. T. Mierke, *Rep. Prog. Phys.* **2019**, *82*, 064602.
[19] D. Barkley, R. Moncada, M. Pour, D. A. Liberman, I. Dryg, G. Werba, W. Wang, M. Baron, A. Rao, B.o Xia, G. S. França, A. Weil, D. F. Delair, C. Hajdu, A. W. Lund, I. Osman, I. Yanai, *Nat. Genet.* **2022**, *54*, 1192.
[20] P. Nallasamy, R. K. Nimmakayala, S. Parte, A. C. Are, S. K. Batra, M. P. Ponnusamy, *Mol. Cancer* **2022**, *21*, 225.
[21] M. V. Liberti, J. W. Locasale, *Trends Biochem. Sci.* **2016**, *41*, 211.
[22] I. Barba, L. Carrillo-Bosch, J. Seoane, *Int. J. Mol. Sci.* **2024**, *25*, 3142.
[23] Y. Wang, G. J. Patti, *Trends Cell Biol.* **2023**, *33*, 1014.
[24] X. Li, S. Yan, J. Dai, Y.i Lu, Y. Wang, M. Sun, J. Gong, Y. Yao, *Colloids Surf., B* **2018**, *162*, 390.
[25] S. Lin, Y. Chai, X. Zheng, X. Xu, *Mol. Biol. Rep.* **2024**, *51*, 14.
[26] E. C. de Heer, M. Jalving, A. L. Harris, *J. Clin. Invest.* **2020**, *130*, 5074.
[27] Y. Luo, Z. Yang, Y. Yu, P. Zhang, *Int. J. Biol. Macromol.* **2022**, *222*, 2225.
[28] C. Jensen, Y. Teng, *Front. Mol. Biosci.* **2020**, *7*, 33.
[29] C. Jubelin, J. Muñoz-Garcia, D. Cochonneau, E. Ollivier, F. Vallette, M.-F. Heymann, L. Oliver, D. Heymann, *Front. Bioeng. Biotechnol.* **2023**, *11*, 1260049.
[30] O. Urzì, R. Gasparro, E. Costanzo, A. De Luca, G. Giavaresi, S. Fontana, R. Alessandro, *Int. J. Mol. Sci.* **2023**, *24*, 12046.
[31] M. Kappelmann-Fenzl, S. K. Schmidt, S. Fischer, R. Schmid, L. Lämmerhirt, L. Fischer, S. Schrüfer, I. Thievessen, D. W. Schubert, A. Matthies, R. Detsch, A. R. Boccaccini, A. Arkudas, A. Kengelbach-Weigand, A. K. Bosserhoff, *Cancers* **2021**, *13*, 111.
[32] A. Jaganathan, J. Toth, X. Chen, L. Pieuchot, Y. Shen, C. Reinhart-King, V. B. Shenoy, *Biophys. J.* **2024**, *123*, 249a.
[33] J. C. Fontoura, C. Viezzer, F. G. dos Santos, R. A. Ligabue, R. Weinlich, R. D. Puga, D. Antonow, P. Severino, C. Bonorino, *Mater. Sci. Eng. C* **2020**, *107*, 110264.
[34] V. Das, F. Bruzzese, P. Konečný, F. Iannelli, A. Budillon, M. Hajdúch, *Drug Discov. Today* **2015**, *20*, 848.
[35] O. E.l Atat, Z. Farzaneh, M. Pourhamzeh, F. Taki, R. Abi-Habib, M. Vosough, M. El-Sibai, *Hum. Cell* **2022**, *35*, 23.
[36] A. Abbott, Nature **2003**, *424*, 861.
[37] A. Tevlek, S. Kecili, O. S. Ozcelik, H. Kulah, H. C. Tekin, *ACS Omega* **2023**, *8*, 3630.
[38] Y. Kang, P. Datta, S. Shanmughapriya, I. T. Ozbolat, *ACS Appl. Bio Mater.* **2020**, *3*, 5552.
[39] R. Onbas, A. Arslan Yildiz, *ACS Appl. Bio Mater.* **2021**, *4*, 1794.
[40] O. Habanjar, M. Diab-Assaf, F. Caldefie-Chezet, L. Delort, *Int. J. Mol. Sci.* **2021**, *22*, 12200.
[41] F. Weiss, N. Atlasy, V. van Reijmersdal, H. Stunnenberg, C. Hulsbergen-Veelken, P. Friedl, *Vitr. Model.* **2022**, *1*, 463.
[42] E. Ko, M. L. S. Poon, E. Park, Y. Cho, J. H. Shin, *ACS Biomater. Sci. Eng.* **2021**, *7*, 3845.
[43] Y. Jeong, A. Tin, J. Irudayaraj, *Front. Bioeng. Biotechnol.* **2022**, *10*, 898699.
[44] V. Härmä, J. Virtanen, R. Mäkelä, A. Happonen, J-P. Mpindi, M. Knuuttila, P. Kohonen, J. Lötjönen, O. Kallioniemi, M. Nees, *PLoS One* **2010**, *5*, e10431.
[45] M. Cavo, D. Delle Cave, E. D'Amone, G. Gigli, E. Lonardo, L. L. del Mercato, *Sci. Rep.* **2020**, *10*, 10192.
[46] J. Aalders, L. Léger, T. Tuerlings, S. Ledda, J. van Hengel, *MethodsX* **2020**, *7*, 101065.
[47] H. Li, P. Liu, G. Kaur, X. Yao, M. Yang, *Adv. Healthcare Mater.* **2017**, *6*, 1700185.
[48] A. Langella, S. D. Gadau, E. Serra, D. Bebbere, S. Ledda, *Biology* **2022**, *11*, 492.
[49] M.o Chen, M. P. Shah, T. B. Shelper, L. Nazareth, M. Barker, J. Tello Velasquez, J. A. K. Ekberg, M-L. Vial, J. A. St John, *ACS Appl. Mater. Interfaces* **2019**, *11*, 9814.
[50] M. Zanoni, M. Cortesi, A. Zamagni, C. Arienti, S. Pignatta, A. Tesei, *J. Hematol. Oncol.* **2020**, *13*, 97.
[51] M. Rimann, S. Laternser, A. Gvozdenovic, R. Muff, B. Fuchs, J. M. Kelm, U. Graf-Hausner, *J. Biotechnol.* **2014**, *189*, 129.
[52] Z. Yuan, Y. Li, S. Zhang, X. Wang, H.e Dou, X.i Yu, Z. Zhang, S. Yang, M. Xiao, *Mol. Cancer* **2023**, *22*, 48.
[53] T. Saydé, O. El Hamoui, B. Alies, K. Gaudin, G. Lespes, S. Battu, *Nanomaterials* **2021**, *11*, 481.
[54] W. H. Abuwatfa, W. G. Pitt, G. A. Husseini, *J. Biomed. Sci.* **2024**, *31*, 7.
[55] D. Wu, Z. Wang, J. Li, Y. Song, M. E. M. Perez, Z. Wang, X. Cao, C. Cao, S. Maharjan, K. C. Anderson, D. Chauhan, Y. S. Zhang, *Adv. Healthcare Mater.* **2022**, *11*, 2100884.
[56] N. C. Negrini, C. Ricci, F. Bongiorni, L. Trombi, D. D'Alessandro, S. Danti, S. Farè, *Cancers* **2022**, *14*, 2003.
[57] Y. T. Tung, Y. C. Chen, K. Derr, K. Wilson, M. J. Song, M. Ferrer, *Adv. Healthcare Mater.* **2024**, *13*, 2302831.
[58] I. Palubeckaite, S. Venneker, I. H. Briaire-de Bruijn, B. E. van den Akker, A. D. Krol, H. Gelderblom, J. V. M. G. Bovée, *Front. Mol. Biosci.* **2020**, *7*, 566291.
[59] K. Unnikrishnan, L. V. Thomas, R. M. Ram Kumar, *Front. Oncol.* **2021**, *11*, 733652.
[60] K. A. G. Katsogiannis, G. T. Vladisavljević, S. Georgiadou, *J. Polym. Sci. B Polym. Phys.* **2016**, *54*, 1878.
[61] X. Zhang, Y. Meng, B. Gong, T. Wang, Y. Lu, L. Zhang, J. Xue, *J. Mater. Chem. B* **2022**, *10*, 7281.
[62] S. Babitha, L. Rachita, K. Karthikeyan, E. Shoba, I. Janani, B. Poornima, K. Purna Sai, *Int. J. Pharm.* **2017**, *523*, 52.
[63] M. Cavo, F. Serio, N. R. Kale, E. D'Amone, G. Gigli, L. L. Del Mercato, *Biomater. Sci.* **2020**, *8*, 4887.
[64] E. Jagtiani, A. S. Sabnis, *Polym. Bull.* **2023**, *80*, 1215.
[65] E. Polonio-Alcalá, M. Rabionet, X. Gallardo, D. Angelats, J. Ciurana, S. Ruiz-Martínez, T. Puig, *Polymers* **2019**, *11*, 916.
[66] C. Ricci, B. Azimi, L. Panariello, B. Antognoli, B. Cecchini, R. Rovelli, M. Rustembek, P. Cinelli, M. Milazzo, S. Danti, A. Lazzeri, *Int. J. Mol. Sci.* **2023**, *24*, 9443.
[67] R. Ramachandran, V. R. Junnuthula, G. S. Gowd, A. Ashokan, J. Thomas, R. Peethambaran, A. Thomas, A. K. K. Unni, D. Panikar, S. V. Nair, M. Koyakutty, *Sci. Rep.* **2017**, *7*, 43271.
[68] J. Wang, Y. Yin, X. Ren, S. Wang, Y. Zhu, *J. Mater. Sci. Mater. Med.* **2024**, *35*, 21.
[69] L. Louis, B. s. Chee, M. McAfee, M. Nugent, *Pharmaceutics* **2023**, *15*, 1649.
[70] K. Furuno, K. Suzuki, S. Sakai, *Biomolecules* **2022**, *12*, 1638.
[71] M. Sepantafar, R. Maheronnaghsh, H. Mohammadi, F. Radmanesh, M. M. Hasani-sadrabadi, M. Ebrahimi, H. Baharvand, *Trends Biotechnol.* **2017**, *35*, 1074.
[72] M. Marzi, M. Rostami Chijan, E. Zarenezhad, *J. Mol. Struct.* **2022**, *1262*, 133014.
[73] A. Zamuner, M. Dettin, L. Dall'Olmo, L. G. Campana, M. E. Mognaschi, M. T. Conconi, E. Sieni, *Bioelectrochemistry* **2024**, *156*, 108624.
[74] P. P. Provenzano, K. W. Eliceiri, J. M. Campbell, D. R. Inman, J. G. White, P. J. Keely, *BMC Med.* **2006**, *4*, 38.
[75] S. Kaur, I. Kaur, P. Rawal, D. M. Tripathi, A. Vasudevan, *Cancer Lett.* **2021**, *504*, 58.
[76] S. S. Soofi, J. A. Last, S. J. Liliensiek, P. F. Nealey, C. J. Murphy, *J. Struct. Biol.* **2009**, *167*, 216.
[77] K. N. Enyedi, G. Enyedi, E. Lajkó, *FEBS Open Bio* **2023**, *13*, 2356.
[78] M. Colasurdo, E. B. Nieves, M. A. Fernández-Yagüe, C. Franck, A. J. García, *Biomaterials* **2022**, *288*, 121710.

[79] S. J. Bidarra, C. C. Barrias, K. B. Fonseca, M. A. Barbosa, R. A. Soares, P. L. Granja, *Biomaterials* **2011**, *32*, 7897.
[80] C. E. Campiglio, S. J. Bidarra, L. Draghi, C. C. Barrias, *Mater. Sci. Eng. C* **2019**, *108*, 110488.
[81] I. M. Savić Gajić, I. M. Savić, Z. Svirčev, *Polymers* **2023**, *15*, 2592.
[82] S. J. Bidarra, P. Oliveira, S. Rocha, D. P. Saraiva, C. Oliveira, C. C. Barrias, *Sci. Rep.* **2016**, *6*, 27072.
[83] S. Grebenyuk, A. Ranga, *Front. Bioeng. Biotechnol.* **2019**, *7*, 39.
[84] J. Majidpoor, K. Mortezaee, *Cell. Oncol.* **2021**, *44*, 715.
[85] F. C. Teixeira, S. Chaves, A. L. Torres, C. C. Barrias, S. J. Bidarra, *Front. Bioeng. Biotechnol.* **2021**, *9*, 647031.
[86] K. B. Pointer, P. A. Clark, A. B. Schroeder, M. S. Salamat, K. W. Eliceiri, J. S. Kuo, *J. Neurosurg.* **2016**, *126*, 1812.
[87] B. Delpech, C. Maingonnat, N. Girard, C. Chauzy, A. Olivier, R. Maunoury, J. Tayot, P. Creissard, *Eur. J. Cancer* **1993**, *29*, 1012.
[88] D. Sood, M. Tang-Schomer, D. Pouli, C. Mizzoni, N. Raia, A. Tai, K. Arkun, J. Wu, L. D. Black, B. Scheffler, I. Georgakoudi, D. A. Steindler, D. L. Kaplan, *Nat. Commun.* **2019**, *10*, 4529.
[89] P. Datta, M. Dey, Z. Ataie, D. Unutmaz, I. T. Ozbolat, *npj Precis. Oncol.* **2020**, *4*, 18.
[90] P. Shukla, S. Yeleswarapu, M. A. Heinrich, J. Prakash, F. Pati, *Biofabrication* **2022**, *14*, 032002.
[91] M. A. Heinrich, W. Liu, A. Jimenez, J. Yang, A. Akpek, X. Liu, Q. Pi, X. Mu, N. Hu, R. M. Schiffelers, J. Prakash, J. Xie, Y. S. Zhang, *Small* **2019**, *15*, 1805510.
[92] N. Ashammakhi, S. Ahadian, C. Xu, H. Montazerian, H. Ko, R. Nasiri, N. Barros, A. Khademhosseini, *Mater. Today Bio.* **2019**, *1*, 100008.
[93] C. Wang, Z. Tang, Y. Zhao, R. Yao, L. Li, W. Sun, *Biofabrication* **2014**, *6*, 022001.
[94] R. Schmid, S. K. Schmidt, R. Detsch, H. Horder, T. Blunk, S. Schrüfer, D. W. Schubert, L. Fischer, I. Thievessen, S. Heltmann-Meyer, D. Steiner, D. Schneidereit, O. Friedrich, A. Grüneboom, H. Amouei, H. Wajant, R. E. Horch, A. K. Bosserhoff, A. Arkudas, A. Kengelbach-Weigand, *Adv. Funct. Mater.* **2022**, *32*, 2107993.
[95] Z. Fan, X. Wei, K. Chen, L. Wang, M. Xu, *Micromachines* **2023**, *14*, 878.
[96] H.-G. Yi, Y. H. Jeong, Y. Kim, Y.-J. Choi, H. E. Moon, S. H. Park, K. S. Kang, M. Bae, J. Jang, H. Youn, S. H.a Paek, D.-W. Cho, *Nat. Biomed. Eng.* **2019**, *3*, 509.
[97] X. Chen, B. Zheng, H. Liu, *Anal. Cell. Pathol.* **2011**, *34*, 5.
[98] T. Cohen Hyams, K. Mam, M. C. Killingsworth, *Micron* **2019**, *130*, 102797.
[99] N. Sun, Y. Jia, S. Bai, Q. Li, L. Dai, J. Li, *Adv. Colloid Interface Sci.* **2023**, *314*, 102880.
[100] D. H. Cho, S. Aguayo, A. X. Cartagena-Rivera, *Biomaterials* **2023**, *303*, 122389.
[101] W. E. Corver, C. J. Cornelisse, *Curr. Diagnostic Pathol.* **2002**, *8*, 249.
[102] S. A. Ghanekar, H. T. Maecker, *Cytotherapy* **2003**, *5*, 1.
[103] L. Saft, *Die Pathol* **2023**, *44*, 164.
[104] A. P. Senft, A. M. LeVine, *Paediatr. Respir. Rev.* **2005**, *6*, 199.
[105] A. T. Manning, J. T. Garvin, R. I. Shahbazi, N. Miller, R. E. McNeill, M. J. Kerin, *Eur. J. Surg. Oncol.* **2007**, *33*, 255.
[106] C. L.e Tourneau, E. Borcoman, M. Kamal, *Nat. Med.* **2019**, *25*, 711.
[107] E. Ahmad, A. Ali, Nimisha, A. Kumar Sharma, F. Ahmed, G. Mehdi Dar, A. Mohan Singh, Apurva, A. Kumar, A. Athar, F. Parveen, B. Mahajan, S. Singh Saluja, *Clin. Chim. Acta* **2022**, *537*, 60.
[108] A. Kindberg, J. K. Hu, J. O. Bush, *Curr. Opin. Cell Biol.* **2020**, *66*, 59.
[109] S. Harmansa, T. Lecuit, *Cells Dev.* **2021**, *168*, 203750.
[110] Q. Zeb, C. Wang, S. Shafiq, L. Liu, *An Overview of Single-Cell Isolation Techniques*, Elsevier Inc, Amsterdam **2019**.
[111] T. Abdelaal, L. Michielsen, D. Cats, D. Hoogduin, H. Mei, M. J. T. Reinders, A. Mahfouz, *Genome Biol.* **2019**, *20*, 194.
[112] S. Y. Park, S. Ter-Saakyan, G. Faraci, H. Y. Lee, *Sci. Rep.* **2023**, *13*, 12093.
[113] M. Massimino, F. Martorana, S. Stella, S. R. Vitale, C. Tomarchio, L. Manzella, P. Vigneri, *Genes* **2023**, *14*, 330.
[114] L. Heumos, A. C. Schaar, C. Lance, A. Litinetskaya, F. Drost, L. Zappia, M. D. Lücken, D. C. Strobl, J. Henao, F. Curion, Single-cell Best Practices Consortium, H. B. Schiller, F. J. Theis, *Nat. Rev. Genet.* **2023**, *24*, 550.
[115] A. Baysoy, Z. Bai, R. Satija, R. Fan, *Nat. Rev. Mol. Cell Biol.* **2023**, *24*, 695.
[116] Y. Hou, H. Yao, J. M. Lin, *J. Pharm. Anal.* **2023**, *13*, 1102.
[117] M. Demicco, X.-Z. Liu, K. Leithner, S.-M. Fendt, *Nat. Metab.* **2024**, *6*, 18.
[118] D. Lähnemann, J. Köster, E. Szczurek, D. J. McCarthy, S. C. Hicks, M. D. Robinson, C. A. Vallejos, K. R. Campbell, N. Beerenwinkel, A. Mahfouz, L. Pinello, P. Skums, A. Stamatakis, C. S. O. Attolini, S. Aparicio, J. Baaijens, M. Balvert, B. D.e Barbanson, A. Cappuccio, G. Corleone, B. E. Dutilh, M. Florescu, V. Guryev, R. Holmer, K. Jahn, T. J. Lobo, E. M. Keizer, I. Khatri, S. M. Kielbasa, J. O. Korbel, et al., *Genome Biol.* **2020**, *21*, 31.
[119] G.-C. Yuan, L. Cai, M. Elowitz, T. Enver, G. Fan, G. Guo, R. Irizarry, P. Kharchenko, J. Kim, S. Orkin, J. Quackenbush, A. Saadatpour, T. Schroeder, R. Shivdasani, I. Tirosh, *Genome Biol.* **2017**, *18*, 84.
[120] S. H. Gohil, J. B. Iorgulescu, D. A. Braun, D. B. Keskin, K. J. Livak, *Nat. Rev. Clin. Oncol.* **2021**, *18*, 244.
[121] M. Jacobo Jacobo, H. J. Donnella, S. Sobti, S. Kaushik, A. Goga, S. Bandyopadhyay, *Sci. Rep.* **2024**, *14*, 3694.
[122] P. Shinde, L. Mohan, A. Kumar, K. Dey, A. Maddi, A. N. Patananan, F.-G. Tseng, H.-Y. Chang, M. Nagai, T. S. Santra, *Int. J. Mol. Sci.* **2018**, *19*, 3143.
[123] K. Pang, S. Dong, Y. Zhu, X.i Zhu, Q. Zhou, B. Gu, W. Jin, R. Zhang, Y. Fu, B. Yu, D.a Sun, Z. Duanmu, X. Wei, *J. Biophoton.* **2023**, *16*, e202300135.
[124] P. P. Austin Suthanthiraraj, S. W. Graves, *Curr. Protoc. Cytom.* **2013**, *65*, 91.
[125] S. P. Perfetto, P. K. Chattopadhyay, M. Roederer, *Nat. Rev. Immunol.* **2004**, *4*, 648.
[126] I. Kanter, T. Kalisky, *Front. Oncol.* **2015**, *5*, 53.
[127] S. Ullas, C. Sinclair, *Int. J. Mol. Sci.* **2024**, *25*, 3851.
[128] Y. Kieffer, H. R. Hocine, G. Gentric, F. Pelon, C. Bernard, B. Bourachot, S. Lameiras, L. Albergante, C. Bonneau, A. Guyard, K. Tarte, A. Zinovyev, S. Baulande, G. Zalcman, A. Vincent-Salomon, F. Mechta-Grigoriou, *Cancer Discov* **2020**, *10*, 1330.
[129] C. Hutton, F. Heider, A. Blanco-Gomez, A. Banyard, A. Kononov, X. Zhang, S. Karim, V. Paulus-Hock, D. Watt, N. Steele, S. Kemp, E. K. J. Hogg, J. Kelly, R.-F. Jackstadt, F. Lopes, M. Menotti, L. Chisholm, A. Lamarca, J. Valle, O. J. Sansom, C. Springer, A. Malliri, R. Marais, M. Pasca di Magliano, S. Zelenay, J. P. Morton, C. Jørgensen, *Cancer Cell* **2021**, *39*, 1227.
[130] R. J. Argüello, A. J. Combes, R. Char, J-P. Gigan, A. I. Baaziz, E. Bousiquot, V. Camosseto, B. Samad, J. Tsui, P. Yan, S. Boissonneau, D. Figarella-Branger, E. Gatti, E. Tabouret, M. F. Krummel, P. Pierre, *Cell Metab.* **2021**, *32*, 1063.
[131] D. Simão, C. M. Gomes, P. M. Alves, C. Brito, *Biotechnol. Adv.* **2022**, *55*, 107883.
[132] L. Lafranchi, D. Schlesinger, K. J. Kimler, S. J. Elsässer, *J. Am. Chem. Soc.* **2020**, *142*, 20080.
[133] D. Saimi, Z. Chen, *Smart Mol.* **2023**, *1*, e20230002.
[134] J. Zhao, Z. Han, C. Xu, L. Li, H. Pei, Y. Song, Z. Wang, B. Tang, *eBioMedicine* **2023**, *90*, 104522.
[135] M. Alieva, M. Barrera Román, S. de Blank, D. Petcu, A. L. Zeeman, N. M. M. Dautzenberg, A. M. Cornel, C. van de Ven, R. Pieters, M. L. den Boer, S. Nierkens, F. G. J. Calkoen, H. Clevers, J. Kuball, Z. Sebestyén, E. J. Wehrens, J. F. Dekkers, A. C. Rios, *Nat. Protoc.* **2024**, *19*, 2052.

[136] P. Kunze, L. Kreiss, V. Novosadová, A. V. Roehe, S. Steinmann, J. Prochazka, C. I. Geppert, A. Hartmann, S. Schürmann, O. Friedrich, R. Schneider-Stock, *Cancers* **2022**, *14*, 2364.
[137] J. Lim, C. Park, M. Kim, H. Kim, J. Kim, D. S. Lee, *Exp. Mol. Med.* **2024**, *56*, 515.
[138] Y. Lin, Y. Yang, K. Yuan, S. Yang, S. Zhang, H. Li, T. Tang, *Bioact. Mater.* **2022**, *18*, 459.
[139] F. Tang, D. Xu, S. Wang, C. K. Wong, A. Martinez-Fundichely, C. J. Lee, S. Cohen, J. Park, C. E. Hill, K. Eng, R. Bareja, T. Han, E. M. Liu, A. Palladino, W. Di, D. Gao, W. Abida, S. Beg, L. Puca, M. Meneses, E. De Stanchina, M. F. Berger, A. Gopalan, L. E. Dow, J. M. Mosquera, H. Beltran, C. N. Sternberg, P. Chi, H. I. Scher, A. Sboner, Y. Chen, E. Khurana, *Science* **2022**, *376*, eabe1505.
[140] L. Gong, J. Luo, Y.u Zhang, Y. Yang, S. Li, X. Fang, B. Zhang, J. Huang, L. K.a-Y. Chow, D. Chung, J. Huang, C. Huang, Q. Liu, L.u Bai, Y. C. Tiu, P. Wu, Y. Wang, G. S. W. Tsao, D. L. W. Kwong, A. W. M. Lee, W. Dai, X.-Y. Guan, *Nat. Commun.* **2023**, *14*, 1912.
[141] S. Lee, H. Kim, B. S. Kim, S. Chae, S. Jung, J. S. Lee, J. Yu, K. Son, M. Chung, J. K. Kim, D. Hwang, S. H. Baek, N. L.i Jeon, *Nat. Commun.* **2024**, *15*, 230.
[142] S. Ding, C. Hsu, Z. Wang, N. R. Natesh, R. Millen, M. Negrete, N. Giroux, G. O. Rivera, A. Dohlman, S. Bose, T. Rotstein, K. Spiller, A. Yeung, Z. Sun, C. Jiang, R. Xi, B. Wilkin, P. M. Randon, I. Williamson, D. A. Nelson, D. Delubac, S. Oh, G. Rupprecht, J. Isaacs, J. Jia, C. Chen, J. P. Shen, S. Kopetz, S. McCall, A. Smith, N. Gjorevski, A.-C. Walz, S. Antonia, E. Marrer-Berger, H. Clevers, D. Hsu, X. Shen, *Cell Stem Cell* **2022**, *29*, 905.
[143] K. Chen, Y. Ma, X. Zhong, J. Lan, D. Long, X. Tian, Y. Yang, Y. Yang, *Cancer Lett.* **2023**, *582*, 216586.
[144] J. Tian, J. H. Chen, S. X. Chao, K. Pelka, M. Giannakis, J. Hess, K. Burke, V. Jorgji, P. Sindurakar, J. Braverman, A. Mehta, T. Oka, M. Huang, D. Lieb, M. Spurrell, J. N. Allen, T. A. Abrams, J. W. Clark, A. C. Enzinger, P. C. Enzinger, S. J. Klempner, N. J. McCleary, J. A. Meyerhardt, D. P. Ryan, M. B. Yurgelun, K. Kanter, E. E. Van Seventer, I. Baiev, G. Chi, J. Jarnagin, et al., *Nat. Med.* **2023**, *29*, 458.
[145] M. Slyper, C. B. M. Porter, O. Ashenberg, J. Waldman, E. Drokhlyansky, I. Wakiro, C. Smillie, G. Smith-Rosario, J. Wu, D. Dionne, S. Vigneau, J. Jané-Valbuena, T. L. Tickle, S. Napolitano, M.-J.u Su, A. G. Patel, A. Karlstrom, S. Gritsch, M. Nomura, A. Waghray, S. H. Gohil, A. M. Tsankov, L. Jerby-Arnon, O. Cohen, J. Klughammer, Y. Rosen, J. Gould, L. Nguyen, M. Hofree, P. J. Tramontozzi, et al., *Nat. Med.* **2020**, *26*, 792.
[146] A. A. Frolova, T. S. Gerashchenko, M. R. Patysheva, A. A. Fedorov, M. M. Tsyganov, U. A. Bokova, O. D. Bragina, M. A. Vostrikova, E. Y.u. Garbukov, N. V. Cherdyntseva, *Bull. Exp. Biol. Med.* **2023**, *175*, 523.
[147] A. Stephenson-Gussinye, L. A. Rendón-Bautista, B. E. Ruiz-Medina, E. Blanco-Olais, R. Pérez-Molina, C. Marcial-Medina, Y. Chavarri-Guerra, E. Soto-Pérez-de-Celis, A. Morales-Alfaro, A. Esquivel-López, F. Candanedo-González, A. Gamboa-Domínguez, R. Cortes-González, A. Alfaro-Goldaracena, S. E. Vázquez-Manjarrez, G. Grajales-Figueroa, B. Astudillo-Romero, J. Ruiz-Manriquez, A. C. Poot-Hernández, P. Licona-Limón, M. Furlan-Magaril, *Front. Mol. Biosci.* **2024**, *11*, 1420308.
[148] J. Zhang, J. Straehle, K. Joseph, N. Neidert, S. Behringer, J. Göldner, A. Vlachos, M. Prinz, C. Fung, J. Beck, O. Schnell, D. H. Heiland, V. M. Ravi, *STAR Protoc.* **2023**, *4*, 102383.
[149] O. Menyhárt, H. Harami-Papp, S. Sukumar, R. Schäfer, L. Magnani, O. de Barrios, B. Győrffy, *Biochim. Biophys. Acta – Rev. Cancer* **2016**, *1866*, 300.
[150] C. Kim, V. Prasad, *JAMA Intern. Med.* **2015**, *175*, 1992.
[151] F. Danzi, R. Pacchiana, A. Mafficini, M. T. Scupoli, A. Scarpa, M. Donadelli, A. Fiore, *Signal Transduct. Target. Ther.* **2023**, *8*, 137.
[152] P. Gilson, J. L. Merlin, A. Harlé, *Cancers* **2022**, *14*, 1384.
[153] V. Jacquemin, M. Antoine, G. Dom, V. Detours, C. Maenhaut, J. E. Dumont, *Cancers* **2022**, *14*, 280.
[154] S. Ramón y Cajal, M. Sesé, C. Capdevila, T. Aasen, L. De Mattos-Arruda, S. J. Diaz-Cano, J. Hernández-Losa, J. Castellví, *J. Mol. Med.* **2020**, *98*, 161.
[155] D. Bedognetti, M. Ceccarelli, L. Galluzzi, R. Lu, K. Palucka, J. Samayoa, S. Spranger, S. Warren, K.-K. Wong, E. Ziv, D. Chowell, L. M. Coussens, D. D. De Carvalho, D. G. DeNardo, J. Galon, H. L. Kaufman, T. Kirchhoff, M. T. Lotze, J. J. Luke, A. J. Minn, K. Politi, L. D. Shultz, R. Simon, V. Thórsson, J. B. Weidhaas, M. L. Ascierto, P. A. Ascierto, J. M. Barnes, V. Barsan, P. K. Bommareddy, et al., *J. Immunother. Cancer* **2019**, *7*, 131.
[156] L. W. Elmore, S. F. Greer, E. C. Daniels, C. C. Saxe, M. H. Melner, G. M. Krawiec, W. G. Cance, W. C. Phelps, *Ca-Cancer J. Clin.* **2021**, *71*, 107.
[157] M. Alieva, A. K. L. Wezenaar, E. J. Wehrens, A. C. Rios, *Nat. Rev. Cancer* **2023**, *23*, 731.
[158] G. Alzeeb, D. Arzur, V. Trichet, M. Talagas, L. Corcos, C. Le Jossic-Corcos, *Sci. Rep.* **2022**, *12*, 1488.
[159] B. Tang, A. Raviv, D. Esposito, K. C. Flanders, C. Daniel, B. T. Nghiem, S. Garfield, L. Lim, P. Mannan, A. I. Robles, W. I. Smith, J. Zimmerberg, R. Ravin, L. M. Wakefield, *Stem Cell Rep.* **2015**, *4*, 155.
[160] A. J. Mannion, *Live Cell Imaging and Analysis of Cancer-Cell Transmigration Through Endothelial Monolayers*, A. V Benest, Ed.: Springer, New York **2022**, p. 329.
[161] M. Wu, A. Neilson, A. L. Swift, R. Moran, J. Tamagnine, D. Parslow, S. Armistead, K. Lemire, J. Orrell, J. Teich, S. Chomicz, D. A. Ferrick, *Am. J. Physiol. Physiol.* **2007**, *292*, C125.
[162] L. Wang, K. Chaudhari, A. Winters, Y. Sun, R. Liu, S.-H. Yang, *J. Cereb. Blood Flow Metab.* **2022**, *42*, 1259.
[163] D. T. H. Leung, S. Chu, *Measurement of Oxidative Stress: Mitochondrial Function Using the Seahorse System*, P. Murthi, and C. Vaillancourt, Eds. Springer, New York **2018**, pp. 285-293.
[164] P. R. Nunes, P. F. Oliveira, I. Rebelo, V. C. Sandrim, M. G. Alves, *Vascul. Pharmacol.* **2024**, *155*, 107372.
[165] G. J. W. van der Windt, C.-H. Chang, E. L. Pearce, *Curr. Protoc. Immunol.* **2016**, *113*, 3.16B.1.
[166] G. Campioni, V. Pasquale, S. Busti, G. Ducci, E. Sacco, M. Vanoni, *Cells* **2022**, *11*, 866.
[167] A. V. Menk, G. M. Delgoffe, *Analyzing Melanoma Cell Oxygen Consumption and Extracellular Acidification Rates Using Seahorse Technology*, K. M. Hargadon, Ed. Springer, New York **2021**, pp. 81-89.
[168] X. Gu, Y. Ma, Y. Liu, Q. Wan, *STAR Protoc.* **2021**, *2*, 100245.
[169] J. Zhang, Q. Zhang, *Methods in Molecular Biology*, H. Pre, M. Haznadar, Ed. Springer, New York **2019**, *1928*, pp. 353.
[170] J. Jiang, D. Huang, Y. Jiang, J. Hou, M. Tian, J. Li, L. Sun, Y. Zhang, T. Zhang, Z. Li, Z. Li, S. Tong, Y. Ma, *Front. Oncol.* **2021**, *11*, 647559.
[171] M. Somova, S. Simm, A. Padmyastuti, J. Ehrdardt, J. Schoon, I. Wolff, M. Burchardt, C. Roennau, P. C. Pinto, *Sci. Rep.* **2024**, *14*, 9357.
[172] E. G. Hunt, K. E. Hurst, B. P. Riesenberg, A. S. Kennedy, E. J. Gandy, A. M. Andrews, C. del Mar Alicea Pauneto, L. E. Ball, E. D. Wallace, P. Gao, J. Meier, J. S. Serody, M. F. Coleman, J. E. Thaxton, *Cell Metab.* **2024**, *36*, 969.
[173] A. J. Walsh, M. C. Skala, *Biomed. Opt. Express* **2015**, *6*, 559.
[174] A. J. Walsh, J. A. Castellanos, N. S. Nagathihalli, N. B. Merchant, M. C. Skala, *Pancreas* **2016**, *45*, 863.
[175] A. A. Gillette, C. P. Babiarz, A. R. VanDommelen, C. A. Pasch, L. Clipson, K. A. Matkowskyj, D. A. Deming, M. C. Skala, *Cancers* **2021**, *13*, 1873.
[176] M. A. Foo, M. You, S. L. Chan, G. Sethi, G. K. Bonney, W.-P. Yong, E. K. H. Chow, E. L.i S. Fong, L. Wang, B.-C. Goh, *Biomark. Res.* **2022**, *10*, 10.

[177] J. T. Sharick, C. M. Walsh, C. M. Sprackling, C. A. Pasch, D. L. Pham, K. Esbona, A. Choudhary, R. Garcia-Valera, M. E. Burkard, S. M. McGregor, K. A. Matkowskyj, A. A. Parikh, I. M. Meszoely, M. C. Kelley, S. Tsai, D. A. Deming, M. C. Skala, *Front. Oncol.* **2020**, *10*, 553.
[178] A. J. Walsh, R. S. Cook, H. C. Manning, D. J. Hicks, A. Lafontant, C. L. Arteaga, M. C. Skala, *Cancer Res.* **2013**, *73*, 6164.
[179] T. M. Cannon, A. T. Shah, M. C. Skala, *Biomed. Opt. Express* **2017**, *8*, 1911.
[180] K. Rattanapornsompong, J. Khattiya, P. Phannasil, N. Phaonakrop, S. Roytrakul, S. Jitrapakdee, C. Akekawatchai, *Biochem. Biophys. Rep.* **2021**, *25*, 100903.
[181] K. Karrobi, A. Tank, M. A. Fuzail, M. Kalidoss, K. Tilbury, M. Zaman, J. Ferruzzi, D. Roblyer, *Sci. Rep.* **2023**, *13*, 3624.
[182] R. Veneziano, T. J. Moyer, M. B. Stone, E.-C. Wamhoff, B. J. Read, S. Mukherjee, T. R. Shepherd, J. Das, W. R. Schief, D. J. Irvine, M. Bathe, *Nat. Nanotechnol.* **2020**, *15*, 716.
[183] Q. Liu, M. Zhao, S. Mytnyk, B. Klemm, K. Zhang, Y. Wang, D. Yan, E. Mendes, J. H. van Esch, *Angew. Chem.* **2019**, *131*, 557.
[184] S. Datta, D. Choudhury, A. Das, D. Das Mukherjee, N. Das, S. S. Roy, G. Chakrabarti, *Tumor Biol* **2017**, *39*.
[185] R. D. Z. Lyles, M. J. Martinez, B. Sherman, S. Schürer, K. L. Burnstein, *PLoS One* **2023**, *18*, 1.
[186] F. Xing, Y.u-C. Liu, S. Huang, X. Lyu, S. M. Su, U.n I.n Chan, P.-C. Wu, Y. Yan, N. Ai, J. Li, M. Zhao, B. K. Rajendran, J. Liu, F. Shao, H. Sun, T. K. Choi, W. Zhu, G. Luo, S. Liu, D.e L.i Xu, K. L. Chan, Q.i Zhao, K. Miao, K. Q. Luo, W. Ge, X. Xu, G. Wang, T.-M. Liu, C.-X. Deng, *Theranostics* **2021**, *11*, 9415.
[187] T. Vicar, M. Raudenska, J. Gumulec, J. Balvan, *Sci. Rep.* **2020**, *10*, 1566.
[188] S. S. Nazari, *Curr. Protoc. Cell Biol.* **2020**, *87*, e105.
[189] S. Randriamanantsoa, A. Papargyriou, H. C. Maurer, K. Peschke, M. Schuster, G. Zecchin, K. Steiger, R. Öllinger, D. Saur, C. Scheel, R. Rad, E. Hannezo, M. Reichert, A. R. Bausch, *Nat. Commun.* **2022**, *13*, 5219.
[190] F. Alemanno, M. Cavo, D. Delle Cave, A. Fachechi, R. Rizzo, E. D'Amone, G. Gigli, E. Lonardo, A. Barra, L. L. del Mercato, *Proc. Natl. Acad. Sci. USA* **2023**, *120*, e2122352120.
[191] R. Rizzo, V. Onesto, S. Forciniti, A. Chandra, S. Prasad, H. Iuele, F. Colella, G. Gigli, L. L. del Mercato, *Biosens. Bioelectron.* **2022**, *212*, 114401.
[192] A. Zargari, G. A. Lodewijk, N. Mashhadi, N. Cook, C. W. Neudorf, K. Araghbidikashani, R. Hays, S. Kozuki, S. Rubio, E. Hrabeta-Robinson, A. Brooks, L. Hinck, S. A. Shariati, *Cell Rep. Methods* **2023**, *3*, 100500.
[193] L. Strbkova, B. B. Carson, T. Vincent, P. Vesely, R. Chmelik, *J. Biomed. Opt.* **2020**, *25*, 086502.
[194] R. Rizzo, V. Onesto, G. Morello, H. Iuele, F. Scalera, S. Forciniti, G. Gigli, A. Polini, F. Gervaso, L. L. del Mercato, *Mater. Today Bio* **2023**, *20*, 100655.
[195] C. Tian, C. Yang, S. L. Spencer, *Cell Rep.* **2020**, *32*, 107984.
[196] B. Holme, B. Bjørnerud, N. M. Pedersen, L. R. de la Ballina, J. Wesche, E. M. Haugsten, *Sci. Rep.* **2023**, *13*, 22982.
[197] V. Onesto, S. Forciniti, F. Alemanno, K. Narayanankutty, A. Chandra, S. Prasad, A. Azzariti, G. Gigli, A. Barra, A. De Martino, D. De Martino, L. L. del Mercato, *ACS Nano* **2023**, *17*, 3313.
[198] K. M. Piltti, B. J. Cummings, K. Carta, A. Manughian-Peter, C. L. Worne, K. Singh, D. Ong, Y. Maksymyuk, M. Khine, A. J. Anderson, *Methods* **2018**, *133*, 81.
[199] X. M. Hu, Z.-X. Li, R.-H. Lin, J.-Q. Shan, Q.-W. Yu, R.-X. Wang, L.-S. Liao, W.-T. Yan, Z. Wang, L. Shang, Y. Huang, Q. Zhang, K. Xiong, *Front. Cell Dev. Biol.* **2021**, *9*, 634690.
[200] D. I. Pattison, M. J. Davies, in *Cancer: Cell Structures, Carcinogens and Genomic Instability*, **2006**, Birkhäuser-Verlag, Basel, Switzerland pp. 131.
[201] L. M. Hirvonen, J. Nedbal, N. Almutairi, T. A. Phillips, W. Becker, T. Conneely, J. Milnes, S. Cox, S. Stürzenbaum, K. Suhling, *J. Biophoton.* **2020**, *13*, e201960099.
[202] A. B. Schroeder, K. B. Pointer, P. A. Clark, R. Datta, J. S. Kuo, K. W. Eliceiri, *J. Biomed. Opt.* **2020**, *25*, 036502.
[203] M. V. Shirmanova, A. I. Gavrina, T. F. Kovaleva, V. V. Dudenkova, E. E. Zelenova, V. I. Shcheslavskiy, A. M. Mozherov, L. B. Snopova, K. A. Lukyanov, E. V. Zagaynova, *Sci. Rep.* **2022**, *12*, 4476.
[204] L.-Y.i Liu, W. Liu, K.-N. Wang, B.o-C. Zhu, X.-Y.u Xia, L.-N. Ji, Z.-W. Mao, *Angew. Chem., Int. Ed.* **2020**, *59*, 9719.
[205] Y. Ouyang, Y. Liu, Z. M. Wang, Z. Liu, M. Wu, *Nano-Micro Lett.* **2021**, *13*, 133.
[206] H. Ranawat, S. Pal, N. Mazumder, *Biomed. Eng. Lett.* **2019**, *9*, 293.
[207] H. Li, J. Yu, R. Zhang, X. Li, W. Zheng, *J. Innov. Opt. Health Sci.* **2019**, *12*, 1930009.
[208] K. König, *Methods Appl. Fluoresc.* **2020**, *8*, 034002.
[209] C. V. Raman, K. S. Krishnan, *Nature* **1928**, *121*, 501.
[210] W. Ji, B. Zhao, Y. Ozaki, *J. Raman Spectrosc.* **2016**, *47*, 51.
[211] G. Pezzotti, *J. Raman Spectrosc.* **2021**, *52*, 2348.
[212] R. R. Jones, D. C. Hooper, L. Zhang, D. Wolverson, V. K. Valev, *Nanoscale Res. Lett.* **2019**, *14*, 231.
[213] H. Shin, S. Oh, D. Kang, Y. Choi, *Adv. Sci.* **2020**, *7*, 1903638.
[214] M. Uematsu, T. Shimizu, *Commun. Biol.* **2021**, *4*, 1176.
[215] E. Wiercigroch, E. Szafraniec, K. Czamara, M. Z. Pacia, K. Majzner, K. Kochan, A. Kaczor, M. Baranska, K. Malek, *Spectrochim. Acta A: Mol. Biomol. Spectrosc.* **2017**, *185*, 317.
[216] J. Xu, T. Yu, C. E. Zois, J.i-X. Cheng, Y. Tang, A. L. Harris, W. E. Huang, *Cancers* **2021**, *13*, 1718.
[217] H. Sato, J. Popp, B. R. Wood, Y. Ozaki, *Raman Spectroscopy in Human Health and Biomedicine*, Taylor and Francis, London **2023**.
[218] S. Ghislanzoni, J. W. Kang, A. Bresci, A. Masella, K. J. Kobayashi-Kirschvink, D. Polli, I. Bongarzone, P. T. C. So, *Biosensors* **2023**, *13*, 973.
[219] D. Lee, J. Du, R. Yu, Y. Su, J. R. Heath, L. Wei, *Anal. Chem.* **2020**, *92*, 13182.
[220] A. Spadea, J. Denbigh, M. J. Lawrence, M. Kansiz, P. Gardner, *Anal. Chem.* **2021**, *93*, 3938.
[221] K. Sofińska, N. Wilkosz, M. Szymoński, E. Lipiec, *Molecules* **2020**, *25*, 561.
[222] G. M. Sommers, M. F. Calegari Andrade, L. Zhang, H. Wang, R. Car, *Phys. Chem. Chem. Phys.* **2020**, *22*, 10592.
[223] A. Hauptmann, G. Hoelzl, M. Mueller, K. Bechtold-Peters, T. Loerting, *J. Pharm. Sci.* **2023**, *112*, 51.
[224] A. Annusová, M. Labudová, D. Truchan, V. Hegedusová, H. Svajdlenková, M. Micusk, M. Kotlár, L. Pribusová Slusná, M. Hulman, F. Salehtash, A. Kálosi, L. Csáderová, E. Svastová, P. Siffalovic, M. Jergel, S. Pastoreková, E. Majková, *ACS Omega* **2023**, *8*, 44497.
[225] Y. Gu, X. Bi, J. Ye, *J. Mater. Chem. B* **2020**, *8*, 6944.
[226] C. García-Astrain, M. Henriksen-Lacey, E. Lenzi, C. Renero-Lecuna, J. Langer, P. Piñeiro, B. Molina-Martínez, J. Plou, D. Jimenez de Aberasturi, L. M. Liz-Marzán, *ACS Nano* **2024**, *18*, 11257.